Geoderma 430 (2023) 116282

Contents lists available at ScienceDirect

Geoderma

journal homepage: www.elsevier.com/locate/geoderma

Soil colloidal particles in a subtropical savanna: Biogeochemical significance and influence of anthropogenic disturbances

Qian Zhang [a,b,*], Thomas W. Boutton [c], Che-Jen Hsiao [c], Ryan M. Mushinski [c,d], Liming Wang [a], Roland Bol [a,e], Erwin Klumpp [a]

[a] Institute of Bio- and Geosciences, Agrosphere (IBG-3), Forschungszentrum Jülich, Wilhelm-Johnen-Str., 52425 Jülich, Germany
[b] Institute for Environmental Research (Biology V), RWTH Aachen University, 52074 Aachen, Germany
[c] Department of Ecology and Conservation Biology, Texas A&M University, College Station, TX 77843, USA
[d] School of Life Sciences, University of Warwick, Coventry CV4 7AL, UK
[e] School of Natural Sciences, Environment Centre Wales, Bangor University, Bangor LL57 2UW, UK

ARTICLE INFO

Handling Editor: Andrew Margenot

Keywords:
Water dispersible colloids
Woody encroachment
Anthropogenic disturbance
Subtropical savanna
Asymmetric flow field-flow fractionation
^{31}P-Nuclear magnetic resonance spectroscopy

ABSTRACT

Soil colloids (diameter < 1000 nm) are comprised mainly of clay minerals and organic matter, and play major roles in determining ion exchange capacity and in regulating key biogeochemical processes. Consequently, it is important to understand how soil colloids and their functions are influenced by land cover and anthropogenic disturbances. In grasslands, savannas, and other dryland ecosystems across the globe, woody plants are encroaching due to livestock grazing, fire suppression, elevated CO_2 concentrations, and climate change. These major land cover changes could influence soil colloidal properties, with implications for soil C, N, and P cycles. We assessed how woody encroachment, livestock grazing, and fire interact to influence soil colloidal properties in a juniper-oak savanna. Surface soils (0–10 cm) from the southern Great Plains (Texas, USA) were collected from long-term treatments differing in grazing intensity (none, moderate, and heavy) and fire history. Within each treatment, soil samples were taken under grass, juniper, and oak canopies. Water dispersible soil colloids (WDC, d < 500 nm) were isolated and analyzed by asymmetric flow field-flow fractionation and their P species by liquid-state ^{31}P-nuclear magnetic resonance spectroscopy (^{31}P NMR). Soil beneath oak and juniper canopies had smaller WDC and elevated colloidal organic carbon (OC) and P concentrations, especially in nanocolloid (<30 nm) and fine colloid (30–160 nm) size fractions. Woody encroachment enriched Ca, Fe, Al, Si and Mg in WDC in the ungrazed control, but not in any of the other grazed or burned areas. Colloidal soil P mainly occurred as orthophosphate and orthophosphate diesters, and was present as OC-Ca-P complexes in fine and medium colloid fractions (30–500 nm), while P in the nanocolloid fraction (<30 nm) was in direct association with Ca. Moderate grazing did not affect the retention of colloidal P, while heavy grazing potentially increased the loss risk of colloidal P. Fire accelerated soil P loss from colloid fractions only in woody areas. Our findings highlight that woody encroachment strengthens the retention of OC and P by soil colloids, consequently increasing overall C and P pools in savanna soils.

1. Introduction

Natural colloidal particles (diameter < 1000 nm) are the smallest particulate phase in soils and consist of organic and inorganic components formed during litter decomposition and mineral weathering (Guggenberger and Haider, 2001; Yan et al., 2018). Some natural colloidal particles can enter the soil solution, potentially enhancing the mobile fraction in soil. The colloid fractions which tend to disperse in water from soil aggregates are referred to as water dispersible colloids (WDC), which can act as potential carriers of nutrients to groundwater (Seta and Karathanasis, 1996). Soil texture (Jiang et al., 2017; Moradi et al., 2020), pH (Sun et al., 2020; Wang et al., 2020; Zhang et al., 2021), organic matter and mineral composition (Krause et al., 2018; Sun et al., 2020), vegetation structure (Missong et al., 2018a), and anthropogenic disturbances (Lekfeldt et al., 2017; Li et al., 2019) all are known to influence soil colloid formation. For example, Jiang et al. (2017) found that nano-sized (1–20 nm) organic matter–Fe/Al–phosphorus (P) colloids were absent in soils with low redox potential (Cambisols) but

* Corresponding author at: Institute of Bio- and Geosciences, Agrosphere (IBG-3), Forschungszentrum Juelich, Germany.
E-mail address: zhangqian90@foxmail.com (Q. Zhang).

https://doi.org/10.1016/j.geoderma.2022.116282
Received 24 March 2022; Received in revised form 13 September 2022; Accepted 18 November 2022

present in soils with high redox potential (Stagnosol).

Natural colloidal particles are commonly regarded as a potential reservoir for soil P, driving P transformation from soil to soil solution where P is more bioavailable (Konrad et al., 2021; Menezes-Blackburn et al., 2021). In contrast to C and N, P limitation is pervasive in highly weathered soils of terrestrial ecosystems, including tropical forests and savannas (Rodrigues et al., 2016; Turner et al., 2018), due to limited source from bedrock weathering (Lang et al., 2016). In mesic temperate ecosystems such as forests and agroecosystems, P is often associated with colloidal organic matter as well as Fe/Al hydroxides (Henderson et al., 2012; Holzmann et al., 2016; Jiang et al., 2015; Li et al., 2021). However, in more arid and semiarid ecosystems, Ca seems to be the key element in colloidal P binding (Moradi et al., 2020; Turner et al., 2004). However, little is known regarding the soil colloidal responses to changes in land cover and use in savanna ecosystem.

Savanna ecosystems cover approximately 20 % of the earth's land surface (Lehmann et al., 2011) and store approximately 30 % of the total carbon (C) present in vegetation and soils globally (Houghton, 2014). Woody plant encroachment into savanna ecosystems is a geographically widespread phenomenon that appears to be driven by fire suppression, livestock grazing, climate change, and rising atmospheric CO_2 concentration (Archer et al., 2017; Boutton et al., 1998; Buitenwerf et al., 2012; Sankaran et al., 2005; Stevens et al., 2017). Woody encroachment generally increases soil organic C, nitrogen (N), and P storage in soils in arid/semi-arid regions (Blaser et al., 2014; Eldridge et al., 2011; Krull et al., 2005; Sitters et al., 2013), which likely increase the source of colloidal OC and P (Krause et al., 2020; Zhang et al., 2021). Furthermore, other soil properties may be altered following woody encroachment, such as porosity (Yu et al., 2018) and hydrologic characteristics (Holdo et al., 2020). Increased porosity, and high water holding capacity can retard soil colloid release (Lekfeldt et al., 2017; Mills et al., 2017). However, it remains unknown how woody encroachment will impact colloid formation and subsequently influence soil C, N, and P storage and dynamics in grasslands, savannas, and other arid and semiarid ecosystems.

Anthropogenic disturbances to savanna ecosystems, particularly grazing and the alteration of fire regimes, also have strong potential to influence nutrient storage in soils. In grasslands and savannas around the world, livestock grazing has been shown to drive changes in: (i) biodiversity of plant and microbial communities, (ii) rates of primary production, (iii) above- vs belowground biomass allocation patterns, (iv) soil chemical and physical properties, and (v) storage and turnover rates of soil C, N, and P (Eldridge et al., 2017; He et al., 2020; Liang et al., 2021; McSherry and Ritchie, 2013; Milchunas and Lauenroth, 1993; Pineiro et al., 2009). The direction and magnitude of these effects do vary with geography, climate, soil type, and grazing management practices (Byrnes et al., 2018; McSherry and Ritchie, 2013; Sanderson et al., 2020). Grazing directly decreases the organic matter input, probably resulting a decrease of colloidal organic matter, such as organic C and P (Li et al., 2021). Moreover, reduced organic matter input probably promotes the release of water dispersible colloids (Lekfeldt et al., 2017). Marquart et al. (2019) reported that a reduction in porosity caused by livestock trampling was counteracted by larger shrubs, and attributed this to the enhanced mass of litter and the increased density of soil surface macropores. At present, little is known in savanna ecosystems regarding the influence of grazing intensity on soil colloidal composition and function.

Similarly, fires in grasslands and savannas can also have significant impacts on C, N, and P storage in soils (Ansley et al., 2006; Holdo et al., 2012; Pellegrini et al., 2018; Pellegrini et al., 2015; Pellegrini et al., 2020). This is due to thermal mineralization, volatilization (Hatten and Zabowski, 2009; Zhao et al., 2012), as well as changes in vegetation structure (Coetsee et al., 2010; Holdo et al., 2012; Pellegrini et al., 2015). Therefore, fires may induce colloid disaggregation as a consequence of the organic matter destruction, or favor strong aggregation when minerals (like Fe/Al oxyhydroxides) recrystallize at high temperatures (Mataix-Solera et al., 2011). However, there is no information on colloid reaction to fire in the encroached savanna.

The purpose of this study was to identify how soil colloids react in a savanna ecosystem experiencing woody plant encroachment and subjected to different grazing intensities and fire regimes. We quantified concentrations of P and other elements in WDC < 500 nm and their size fractions in relation to vegetation cover type, livestock grazing, and prescribed fire by using asymmetric flow field-flow fractionation. The P species were characterized by ^{31}P NMR. We hypothesized that: (i) besides Fe/Al (hydr)oxides, Ca also can be a critical adhesive in colloidal P retention in savanna ecosystems; (ii) colloidal OC and P increase in line with total organic matter accrual in bulk soils during woody encroachment; and (iii) colloid formation and related P retention are hindered by grazing and fire.

2. Materials and methods

2.1. Site description

Field research was conducted at the Texas A&M AgriLife Sonora Research Station (30° 15′ 59″ N; 100° 33′ 57″ W) located in Texas, USA, on the western edge of the Edwards Plateau. The site has a dry-subhumid climate, with a mean annual temperature of 17.9° C, and mean annual precipitation of 586 mm. Surface soils are silty clays and clays of the Tarrant series (clayey-skeletal, smectitic, thermic Lithic Calciustolls) (USDA/NRCS, 2015). Bedrock is indurated limestone from the Lower Cretaceous. Soil properties (pH, texture, and concentrations of C, N, and P) for the study area are summarized in Table S1.

Vegetation in the study area consists of a grassland matrix dominated by the grasses *Hilaria belangeri*, *Bouteloua curtipendula*, *Nassella leucotricha*, and *Aristida* spp.; patches of woody plants dominated by *Quercus virginiana* (live oak) and *Juniperus ashei* are scattered throughout the grassy matrix (Smeins et al., 1976; Taylor et al., 2012). *Juniperus ashei* appears to have increased dramatically in the grasslands of the Edwards Plateau region during the past century (Fuhlendorf and Smeins, 1997; Jessup et al., 2003).

This region was heavily grazed by cattle, sheep, and goats beginning around 1880. In 1948, the Sonora Research Station implemented several long-term grazing treatments that have been maintained up to the present: (i) an 11 ha control where grazing was excluded, (ii) a 24 ha moderately grazed site, and (iii) a 7 ha heavily grazed site. Stocking rates for the moderately grazed area were 6–8 ha/animal unit/yr, while those for the heavily grazed site were 2–5 ha/animal unit/yr. The ratio of cattle:sheep:goats in the grazed areas has been approximately 60:20:20 since 1948 (Marshall, 1995). None of these grazing treatments have experienced fire since their establishment in 1948, and it is unlikely that they have burned since approximately 1880.

In addition to the grazing treatments, we sampled another experimental area (10 ha) where winter-spring fires were applied every other year from 1986 to the present. As with the grazing treatments, it is unlikely that this fire treatment site experienced any fires from 1880 to 1986. The ungrazed control treatment described in the previous paragraph also served as a control for the fire treatment since it had not experienced fire since about 1880, it was on the same soil type, and it was in close physical proximity (0.5 km) to the fire treatment.

2.2. Field sampling

In each of the grazing and fire treatments described above, soil samples were collected from three portions of the landscape: (i) open grasslands ($n = 3$), (ii) juniper woodlands ($n = 3$), and (iii) oak mottes ($n = 3$). Each sample was a composite mixture of bulk topsoil (0–10 cm) derived from three subsamples, each obtained from a 0.1 m^2 quadrat located within an area of approximately 4 m^2. Soils were stored frozen within 5 h of field collection.

2.3. Water dispersible colloids (WDC) extraction

The WDC extraction was based on the protocol of Séquaris and Lewandowski (2003). Soils were air dried and sieved to 2 mm to remove stones and large organic particles. Then, 50 g of soil were mixed with 100 mL Milli-Q water, horizontally shaken at 150 rpm for 6 h, and mixed with an additional 300 mL of water before sedimentation. Sedimentation time was calculated (27 h) for the desired particle size by Stoke's law (Section S1), based on the bottle size and water height (105 mm) in the bottle. Following sedimentation, the non-settling supernatant phase (including solutes and particles < 2 μm) was centrifuged (Biofuge, Heraeus, Hanau, Germany) for 10 min at 6000 g to obtain the desired colloids < 500 nm. The centrifugation time was calculated by Hathaway (1956) (Section S1). The 30 mL of final supernatant containing solutes and WDC (d < 500 nm) was the water extractable phase (WEP), and was refrigerated prior to field-flow fractionation. The remaining 300 mL supernatant was centrifuged again at 20,000 g for 4 h to separate the 30–500 nm colloid fraction from the "aqueous phase" fraction (including solutes and < 30 nm nanocolloids). Then both fractions were lyophilized for ^{31}P-Nuclear Magnetic Resonance spectroscopy (^{31}P NMR) measurement. Note that for each element, WEP concentration is the sum of water dispersible colloids-associated and the dissolved element concentration (Javidpour et al., 2009). The WDC concentration was determined from the WEP by using asymmetric flow field-flow fractionation.

2.4. Asymmetric flow field-flow fractionation

The nanocolloids and colloids were size separated using asymmetric flow field-flow fractionation (AF2000, Postnova Analytics, Landsberg, Germany). The field-flow fractionation was coupled online to a UV detector (Postnova Analytics, Landsberg, Germany), a dynamic light scattering detector (DLS; Malvern Instruments), an organic carbon detector (OCD; DOC laboratory Dr. Huber, Germany) and an inductively coupled plasma mass spectrometer (ICP-MS; Agilent 7500, Agilent Technologies, Santa Clara, California). The OC, P, Fe, Al, silicon (Si), Ca, and manganese (Mn) concentrations in the WDC fractions were determined by OCD and ICP-MS, respectively. The concentration of each element was converted from OCD or ICP-MS signals. Internal and external standards were added for the measurement and quantitative analysis. Further details of the field-flow fractionation technique and analytical element determination are described in Giddings (1993) and Schimpf et al. (2000). Details concerning the parameters of the separation method based on the previous experience (Missong et al., 2018a) are shown in Table S2.

2.5. ^{31}P-Nuclear magnetic resonance spectroscopy

In order to extract a wide range of organic P (P_o) and inorganic P (P_i) compounds, the procedure of Cade-Menun and Preston (1996) was used. In brief, 0.5 M NaOH and 0.1 M EDTA (Merck) were mixed in a volume ratio of 1:1. We extracted the 2 mm sieved soils, 30–500 nm lyophilized colloids as well as the lyophilized "aqueous phase" (containing solutes and nanocolloids < 30 nm) with the EDTA + NaOH reagent in a w:V ratio 1:10. The samples were shaken for 16 h on a horizontal shaker at 150 rotations min^{-1}, then centrifuged at 10,000 g for 30 min to extract the supernatant, which was lyophilized subsequently. Approximately 100 mg of each lyophilized material was dissolved in pH 13 matrix (0.1 mL 30 % NaOD mixed with 7.4 mL D_2O), and added with methylenediposphonic acid (MDPA, 0.84 mg/mL in pH 13 matrix) reference standard solution, then vortexed and centrifuged at 14,000 g for 30 min. The supernatant was transferred into an NMR tube for the ^{31}P NMR measurement. The ^{31}P NMR measurements were performed on a Varian 600 MHz spectrometer (Varian, Palo Alto, California USA) equipped with a 5 mm broadband probe tuned to the ^{31}P nucleus using methods described elsewhere (Wang et al., 2020). Briefly, the parameters were set as: 45° pulse calibrated at 6.0 μs, 0.4 s acquisition time, 5 s total relaxation delay, 15,800 scans, proton inverse gated decoupling, and a temperature of 293.15 K.

The ^{31}P NMR data analysis was conducted with the MestReNova Software (Mestrelab Research S.L., version 13). The phase and baseline correction as well as the signal assignment of phosphonate, orthophosphate, monoesters, diesters and pyrophosphate was based on previous work (Cade-Menun, 2015; Smernik et al., 2015), and their quantification analysis was conducted based on the ratios of their peak areas to the standard peak area (set as 17.5 ppm).

2.6. Data analyses

The original eluting time of field-flow fractionation was converted to colloid size by comparing the time in DLS fractogram, and the eluting time in field-flow fractionation fractogram. The raw data of the ICP-MS measurements were collected in counts per second with the ICP-MS MassHunter Workstation Software (Agilent Technologies, Santa Clara, California, USA). The raw data of OCD were collected in volts of the detector signal with the field-flow fractionation analytical software (Postnova, Landsberg, Germany). The raw data were exported to Excel® (Microsoft Corporation, Redmond, USA). The peak areas of the separated particle size fractions were integrated and converted to concentration in nmol by means of linear, multipoint calibration. Finally, the results were transformed into μg kg_{soil}^{-1} considering the water content of the samples and the extracted sample weight. One-way ANOVA tests for vegetation type and treatment, and two-way ANOVA tests for their interaction as well as Waller-Duncan T test ($p < 0.05$) were conducted to exam the statistical differences in SPSS (IBM, version 26, Armonk, New York, USA).

To identify the preferential binding partners among the distributed elements, hierarchical tree cluster analysis was applied for each particle size fraction across all sample sites (Gottselig et al., 2017). The distances are given as 1 – Pearson's coefficient, and the complete linkage rule applies for the distance analysis. Thus, the lower the distance, the bigger the occurrence of associations between the elements.

3. Results

3.1. Linkage between P and other elements in WDC size fractions

The particle size related peaks and trend in the OC fractogram of WDC matched those of P and Ca, but differentiated from Al, Si, Fe and Mg (Fig. 1 and S4). Clearly, OC (8–120 mg kg_{soil}^{-1}) dominated in all samples, following by Si, Ca and Al (0.4–12.0 mg kg_{soil}^{-1}), then Fe, Mg and P (0.1–3.8 mg kg_{soil}^{-1}) (Fig. 2a). The fractograms show that OC, P and Ca signals at the first peak of WDC were about 1.5–6 times higher in the oak soil samples compared to grassland (Fig. 1). Their signals in the juniper soil samples were generally intermediate between oak and grassland samples (Fig. S2). The WDC fractogram for OC was dominated by a single peak in the nanocolloids fraction, but with a large shoulder covering fine colloids and to a lesser extent the medium colloids fraction. For OC, P and Ca, the dominant peaks were always related to particle size (Figs. 1 and S4), and were independent of management (control, moderate and heavy grazing, fire) or vegetation type. Furthermore, the proportions of nanocolloidal OC, P and Ca were higher under oaks than under grasslands in every grazing treatment, but there was a decrease in medium colloids and no obvious change in fine colloids (Fig. 2b). Fire significantly reduced the OC and P concentrations in total WDC of oak encroached sites compared to control, especially P in nanocolloids (Figs. 1 and 2a). The interaction of vegetation type and treatment did not show an obvious effect on OC and Ca concentrations in total WDC (Fig. S3).

For Al, Si, Fe and Mg, the WDC fractogram started with a small but sharp peak in the nanocolloids fraction, through one or two wider peaks in fine colloids and finally reached a dominating peak in medium

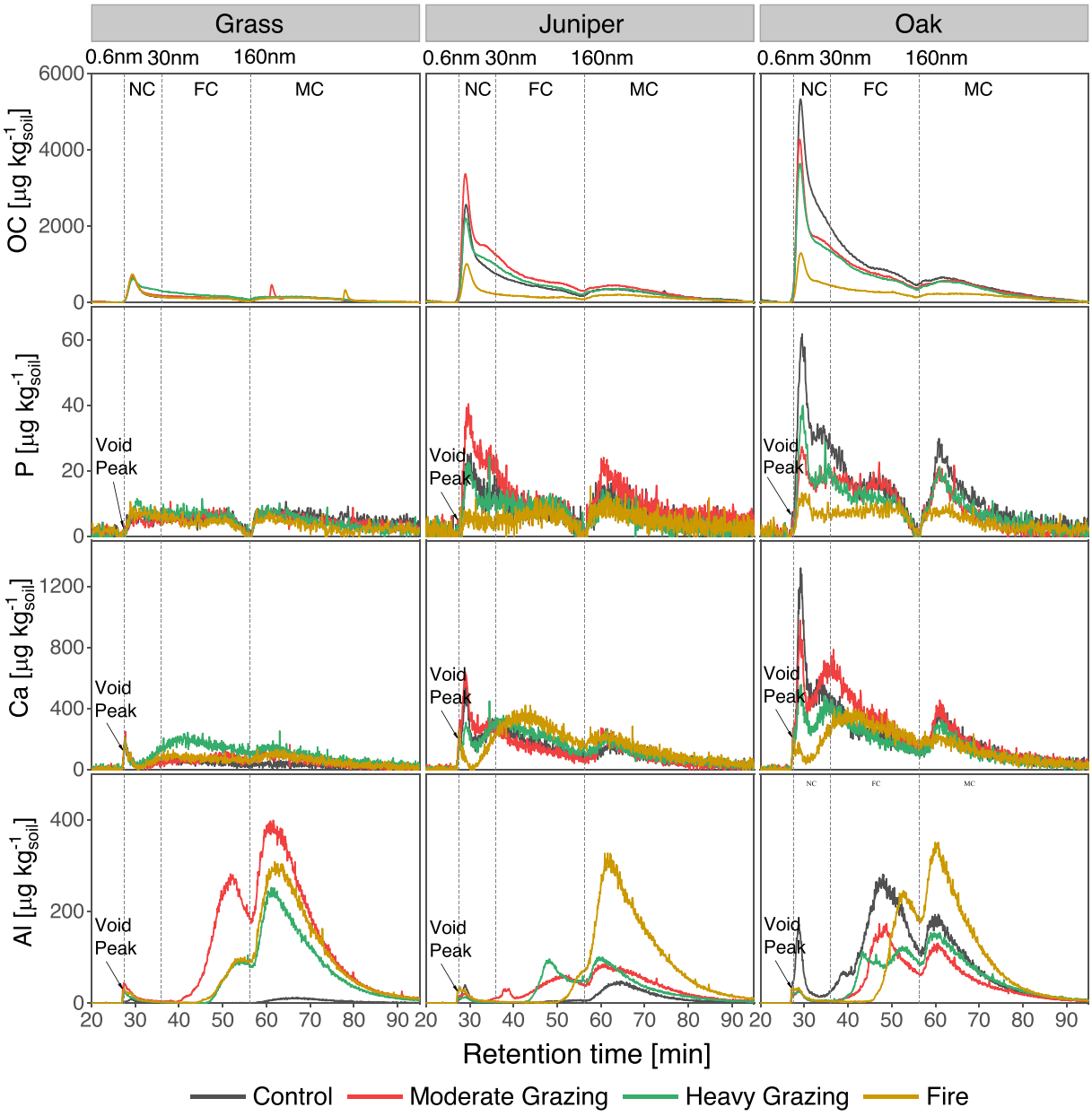

Fig. 1. Soil organic C, P, Ca, and Al concentration in water dispersible colloids (WDC) beneath grass, juniper, and oak with different treatments. Treatments included control, moderate grazing, heavy grazing and fire. The retention time in the x-axis indicated particle size. Nanocolloids (NC), 0.6–30 nm; Fine colloids (FC), 30–160 nm; Medium colloids (MC), >160 nm. One from every-three replicates was selected for the figures. All three replicates showed the same overall pattern in size fractions. Fractograms of other elements are showed in Fig. S2.

colloids fraction (Figs. 1 and S4). The differences in the colloidal size fraction peaks were apparent between vegetation types and land management. Sub-peaks emerged in fine colloids fraction when grassland was encroached by juniper and oak (Figs. 1 and S4), meanwhile the nano-, fine and medium colloidal Al, Si, Fe and Mg concentrations significantly increased (see control grass, juniper and oak sites in Figs. 2 and S5). Grazing and fire, compared to control, increased their values in grassland, but the differences were eliminated when juniper and oak encroached (Fig. S3). Furthermore, the proportions of Al, Si, Fe, and Mg in fine colloids fraction significantly ($p < 0.05$) increased, while that in medium colloids decreased when grasslands were encroached by juniper and oak, and the effects of vegetation type were independent of management methods (Fig. 2b). In grassland, grazing and fire increased the relative proportions of Si, Al, and Fe in fine colloids fraction. In soils beneath juniper, grazing elevated their proportions in fine colloids but reduced the values in medium colloids, while fire affected reversely. In oak encroached soil, heavy grazing and fire visually reduced their proportions in fine colloids fraction while moderate grazing did not affect the ratios.

The 1 - Pearson's coefficient (r) indicate that P clustered with Ca, Mg and Fe in the first fraction (<30 nm nanocolloids) (Fig. 3a), and with OC and Ca in the second (30–160 nm fine colloids) and third fractions (160–500 nm medium colloids) (Fig. 3b and c). Al, Si, Fe and Mg strongly associated with each other in fine and medium colloids fractions, with the 1 - Pearson's r distance diminishing from fine colloids fraction to medium colloids fraction (Fig. 3b and c).

3.2. *Phosphorus and organic carbon in water extractable phase and water dispersible colloids*

The P (Fig. 4a) and OC (Fig. 4c) concentrations in WDC and WEP were significantly ($p < 0.05$) lower in the grassland soils than those

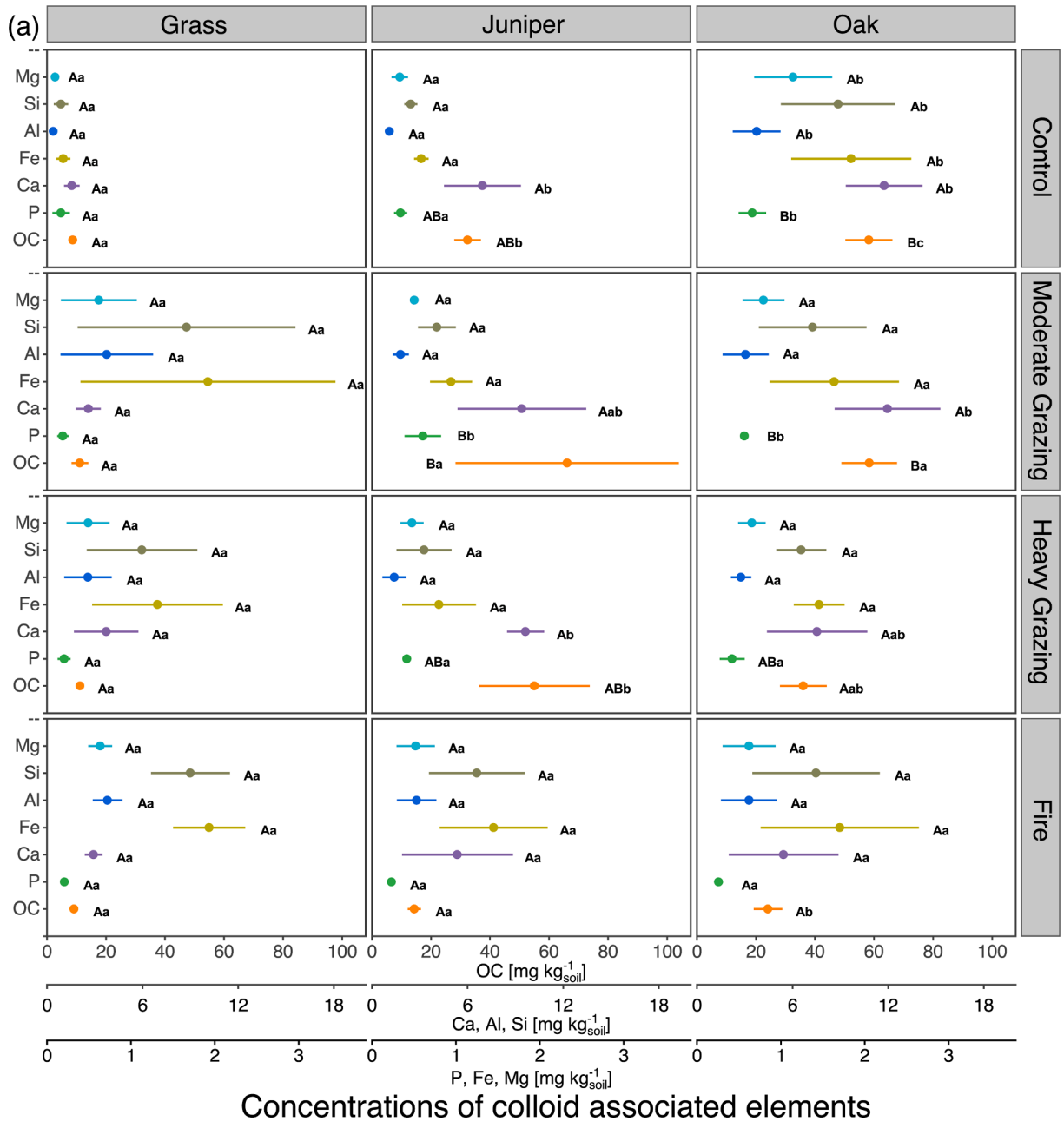

Fig. 2. Concentrations of the elements in WDC (a) and proportions of elements (b) distributed in different size colloids. Nanocolloids: 0.6–30 nm; Fine colloids: 30–160 nm; Medium colloids: 160 nm−500 nm. Values are means ± standard deviations (N = 3). Capital letters and lowercases represent difference between treatments and vegetation type, respectively ($p < 0.05$).

under woody plants. Regardless of vegetation cover, fire diminished ($p < 0.05$) both their WDC and WEP concentrations compared to other three treatments (Fig. 4b & d).

The WDC/WEP ratio was computed as an index of transportable elements. Higher WDC/WEP ratios indicate a lower relative contribution of dissolved elements. The WDC/WEP for P increased significantly ($p < 0.05$) from the oak sites to the grasslands (Fig. 4a). However, differences of WDC/WEP for P between management and their interaction with vegetation types were not significant (Fig. 4b). Moreover, WDC/WEP of P (0.30–1.08) exceeded that of OC (0.19–0.29).

3.3. Phosphorus speciation in bulk soil and water dispersible colloids

Higher total soil P concentrations did not necessarily lead to more colloidal P (P associated with 30–500 nm colloids) or "aqueous phase" P (including the P associated with < 30 nm colloids) (Fig. 5a). For instance, the most abundant soil total P (292 mg P kg^{-1}_{soil}) was in the moderately grazed juniper site, while the most colloidal P (0.86 mg P kg^{-1}_{soil}) was found in the control oak site, and the most "aqueous phase" P (1.18 mg P kg^{-1}_{soil}) in heavily grazed grassland. Moreover, control grassland contained the least colloidal P (0.14 mg P kg^{-1}_{soil}) and "aqueous phase" P (0.14 mg P kg^{-1}_{soil}) although it contained abundant soil total P (108 mg P kg^{-1}_{soil}).

Generally, a higher proportion of P_i (including orthophosphate and pyrophosphate) occurred in the 30–500 nm sized colloids (30–65 %) than in bulk soil (16–27 %) (Fig. 5b). For P_o, orthophosphate monoester dominated in bulk soil (59–73 %), but it was dramatically diminishing in colloids (6–14 %) and in some cases in the "aqueous phase" (2–64 %). In

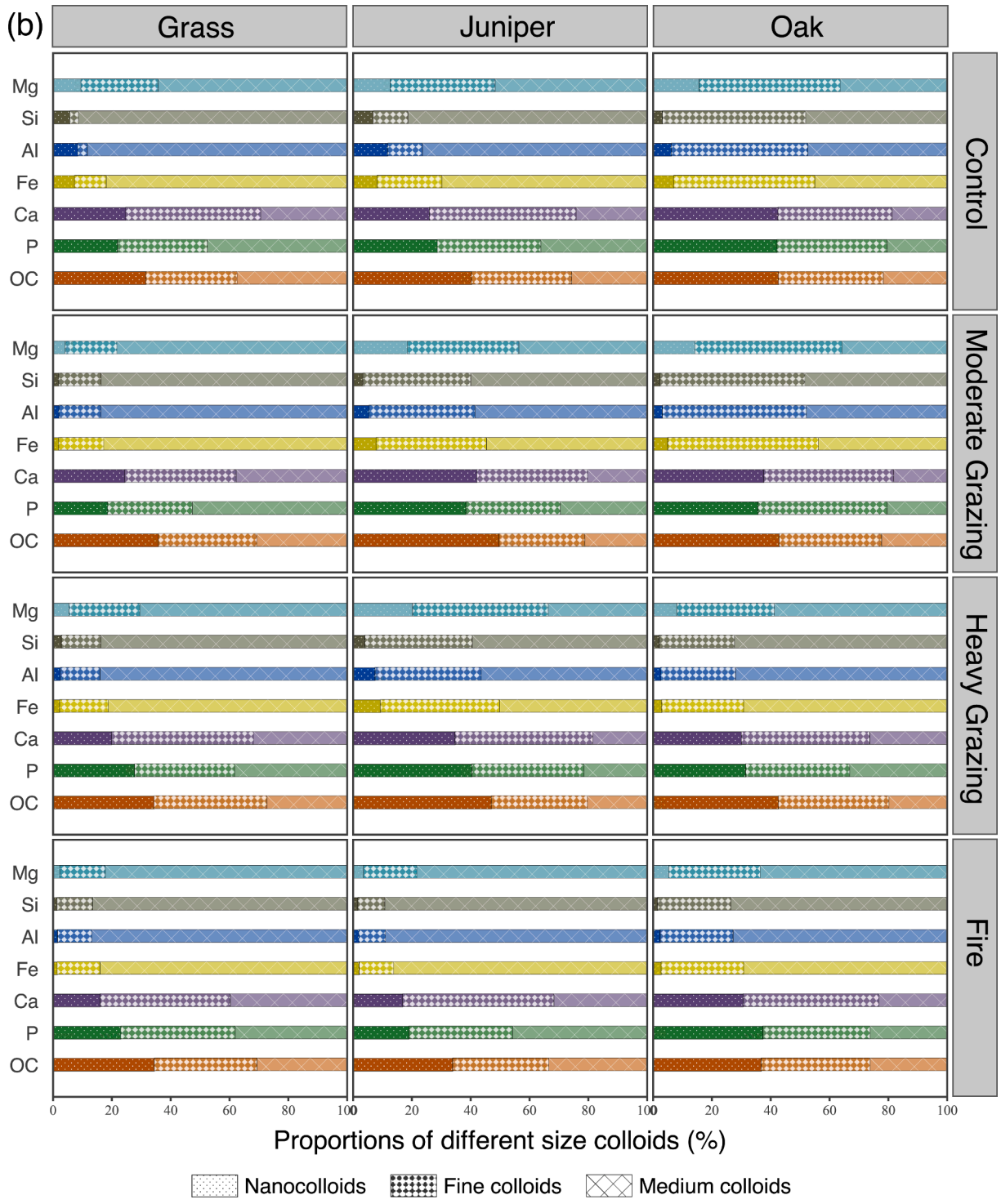

Fig. 2. (*continued*).

contrast, the relative proportion of orthophosphate diester increased sharply from bulk soil (8–17 %) to 30–500 nm colloid (28–55 %) and in some cases to "aqueous phase" (2–54 %). Furthermore, a higher proportion of phosphonate was present in 30–500 nm colloids and the "aqueous phase" compared to bulk soil (Fig. 5b). Orthophosphate proportion slightly increased between grass (14–20 %) to juniper (21–25 %) and oak (18–25 %) vegetation in the bulk soils, but decreased in 30–500 nm colloids (from 35 to 60 % in grassland to 22–37 % in oak site) and the "aqueous phase" (from 35 to 93 % in grassland to 0–35 % in oak site). From a management perspective, heavy grazing (18–93 %) and particularly fire (35–82 %) sharply increased orthophosphate proportions in the "aqueous phase". However, the differences of orthophosphate, orthophosphate diester and orthophosphate monoester proportions in 30–500 nm colloids between moderate vs heavy grazing treatments were not clear.

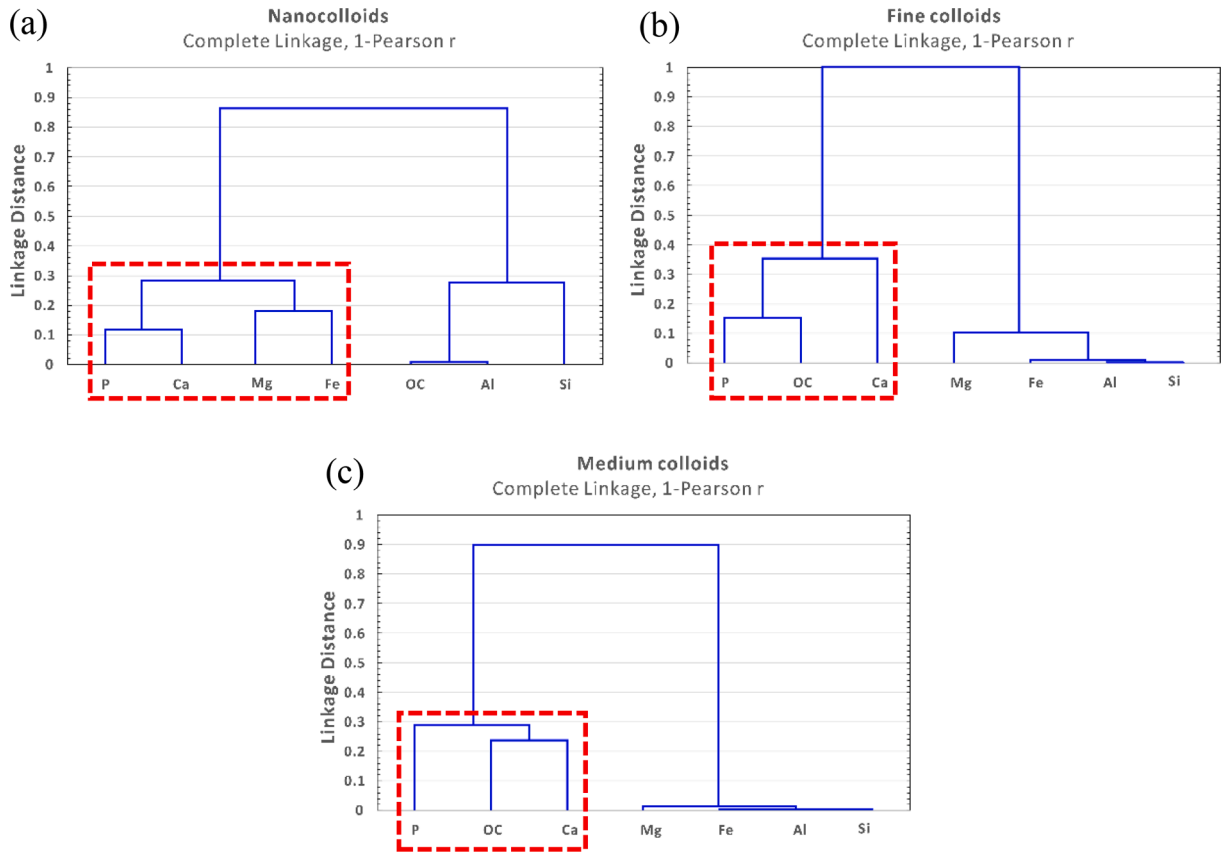

Fig. 3. Hierarchical tree clusters for preferential binding partners in nanocolloid fractions (a), fine colloid fractions (b) and medium colloid fractions (c) across all sample sites. The height of the boxes equals the 1 – Pearson's coefficient (r) distance. The complete linkage rule applies for the analysis. The lower the distance, the stronger the occurrence of associations between the elements. Nanocolloid fractions (NC): 0.6–30 nm; Fine colloid fractions (FC): 30–160 nm; Medium colloid fractions (MC): >160 nm.

4. Discussion

4.1. Water dispersible colloids constituents in soils

The clay minerals in the study areas are likely phyllosilicates with some Fe and/or Mg isomorphic substitutions, evidenced by the Si to Al ratios of 2:1 across all treatments in WDC and the clustered Fe and Mg (Fig. 3) (Tsiantos et al., 2018). SOC was more dominant in nanocolloids fraction than in fine and medium fractions (Fig. 1), suggesting the specific role of nanocolloids for SOC association (Missong et al., 2018a; Wang et al., 2020). In the nanocolloids fraction, SOC clustered strongly with Al, indicating the association of OC with Al species (Fig. 3a). The SOC dominance in nanocolloids was also reported by other studies (Krause et al., 2020; Missong et al., 2018a).

Due to the solubility of limestone and the alkaline environment, Ca^{2+} is particularly enriched in soil water of calcareous soils. Studies of grasslands occurring on limestone bedrock (Li et al., 2017; O'Brien et al., 2015) generally show a positive correlation between SOC and exchangeable Ca^{2+} concentration. The Ca^{2+} cation can act as bridge to connect SOC, negatively charged P species and minerals (Dlamini et al., 2019; Rowley et al., 2021; Rowley et al., 2018) in the WDC (Wang et al., 2020; Zhang et al., 2021). Furthermore, $CaCO_3$ colloids like calcite are positively charged below pH 8 (Somasundaran and Agar, 1967) and can bind SOC and P species. Phosphorus in nanocolloid fractions (Fig. 3a) was deemed reasonably to cluster with Ca, Mg and Fe via charge interactions. In the FC and medium colloids fractions of the studied WDC, P tightly clustered with OC and Ca (Fig. 3b and c), indicating that P can be present as organic P or as P species like orthophosphate attracted to organic substances via Ca^{2+} bridges (Wang et al., 2020). Therefore, our first hypothesis was confirmed namely, that Ca is the critical adhesive in colloidal P retention in our savanna soils.

The orthophosphate monoester fraction is derived from litter degradation, and accounted for most of soil total P in all bulk soils studied (Missong et al., 2016; Wang et al., 2020), followed by orthophosphate and orthophosphate diester. Compared to the dominance of orthophosphate monoester in bulk soil, the observed enrichment of orthophosphate and orthophosphate diester in 30–500 nm colloids revealed their tendency to be adsorbed or occluded by WDC. Orthophosphate, the dominant P_i form in the colloidal fraction, exists as an anion dissolved in "aqueous phase". It preferably binds to the negatively charged surface of soil colloids like clay minerals through cation bridging, or to the positively charged colloids such as iron oxides via electrostatic interaction (Jiang et al., 2015; Missong et al., 2018a; Pang et al., 2016).

4.2. Woody encroachment effect on WDC elements

In our study, colloidal OC and P concentrations were higher under oak compared to grassland (Fig. 2a) in the Edwards Plateau region. The mass percentages of WEP (Fig. S1) also increased following woody encroachment for the control area. It is therefore likely that SOC and P accumulate in bulk soil as a result of the higher SOC inputs and slower decomposition rates of woody plant litter in the encroached soil (Bendevis et al., 2010; Leitner et al., 2018; Liao et al., 2006).

In areas encroached by woody plants in the control plot, the nanocolloid fraction was more enriched in OC, P, Ca, and Mg than either fine or medium colloids. Following the decomposition of litter, the negatively charged P species and SOM are enriched in the nanocolloid fraction, and likely associate by cation bridges of Ca^{2+} and Mg^{2+} as well as the positively charged Fe/Al(hydr)oxide and $CaCO_3$ nanoparticles

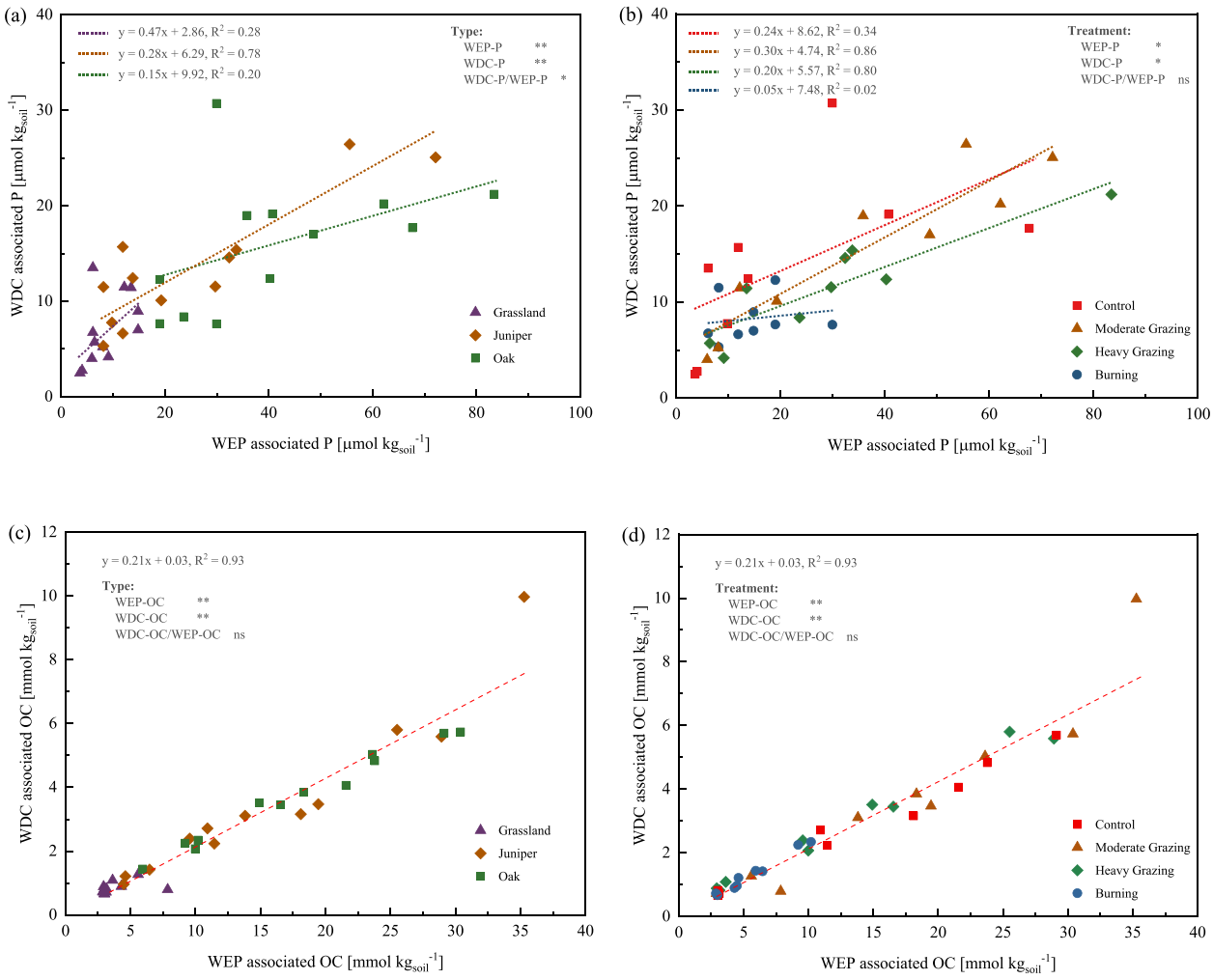

Fig. 4. Linear regression analyses between the water dispersible colloids-associated (WDC) concentration and the water extractable phase (WEP) concentration for phosphorus (a, b) and organic carbon (c, d) by different vegetation types and treatments. WEP content is the total amount of WDC content with dissolved phase content. One-way ANOVA (p-value) tests for vegetation type and treatment, and two-way ANOVA (p-value) tests for their interaction were conducted to examine the effects: * indicates $p < 0.05$; ** indicates $p < 0.01$; ns indicates no significant difference. Results of two-way ANOVAs (p-values) examining the interactions are: WEP-P ns, WDC-P ns, WDC-P/WEP-P ns; WEP-OC *, WDC-OC ns, WDC-OC/WEP-OC ns.

(Schwertmann and Fechter, 1982; Somasundaran and Agar, 1967; Wang et al., 2020). Similar findings in previous studies (Krause et al., 2020; Missong et al., 2018a; Zhang et al., 2021) suggest that higher SOM concentrations favor the formation of nano-colloids. This corroborated our second hypothesis that both colloidal OC and P increase in line with their general accumulation in bulk soils during woody encroachment. Noteworthy, the amount of colloids generally increased during woody encroachment. This finding can be attributed to the colloid stabilization by the negatively charged molecules deriving from lignin decomposition in the woody encroached soils.

The significant difference of the ratio WDC-P/WEP-P among vegetation types indicated that the adsorption effect of colloids on P was weakened with woody encroachment, but the dissolution of P from soil was favored, resulting in greater bioavailability of soil P for plants and microorganisms. This might be due to the fact that the increased organic matter concentrations in encroached areas is occupying the surface adsorption sites of clay particles, weakening their adsorption capacity for P (Li et al., 2021; Missong et al., 2018b; Siemens et al., 2008).

Both P_i and P_o concentrations increased in bulk soil and colloids following woody encroachment in the control area (Fig. 5a). This may be due to the increased SOM input (Rossatto and Rigobelo, 2016; Zhou et al., 2018) as well as the generally larger and more active soil microbial biomass compartment in soils beneath woody plants in savannas, as documented previously at this site (Marshall, 1995) and at other sites in the Great Plains and elsewhere around the world where woody plants are encroaching into grassland (Eldridge et al., 2011; Farella et al., 2020; George et al., 2018; Liao and Boutton, 2008; McCulley et al., 2004). As the main plant in the intermediate stages of encroachment, the effect of juniper laid generally intermediate between oak and grass. The proportion of P_i in the "aqueous phase" (which contained the nanocolloids < 30 nm) generally declined in encroached soils in the control (Fig. 5b). This can mainly be attributed to a relatively excessive consumption of soluble P_i during the growth of juniper and oak. Another reason could be the P_i sorption uptake of increased amounts of colloids, especially the fine or medium colloids fractions, which mainly consist of SOM and clay minerals. Additionally, larger mass of P_o input and P_i consumption by increased plant mass in oak encroached soils apparently promoted the presence of P_o in the "aqueous phase" and colloids as shown in Fig. 5.

4.3. Grazing effect on WDC elements

Consumption of vegetation by livestock and its conversion into excreta with high OC, N and P concentrations are the two additional pathways for element cycling in the grazed treatment areas compared to the ungrazed control (Sitters et al., 2020). Our study revealed that moderate grazing did not affect elemental concentrations in WDC

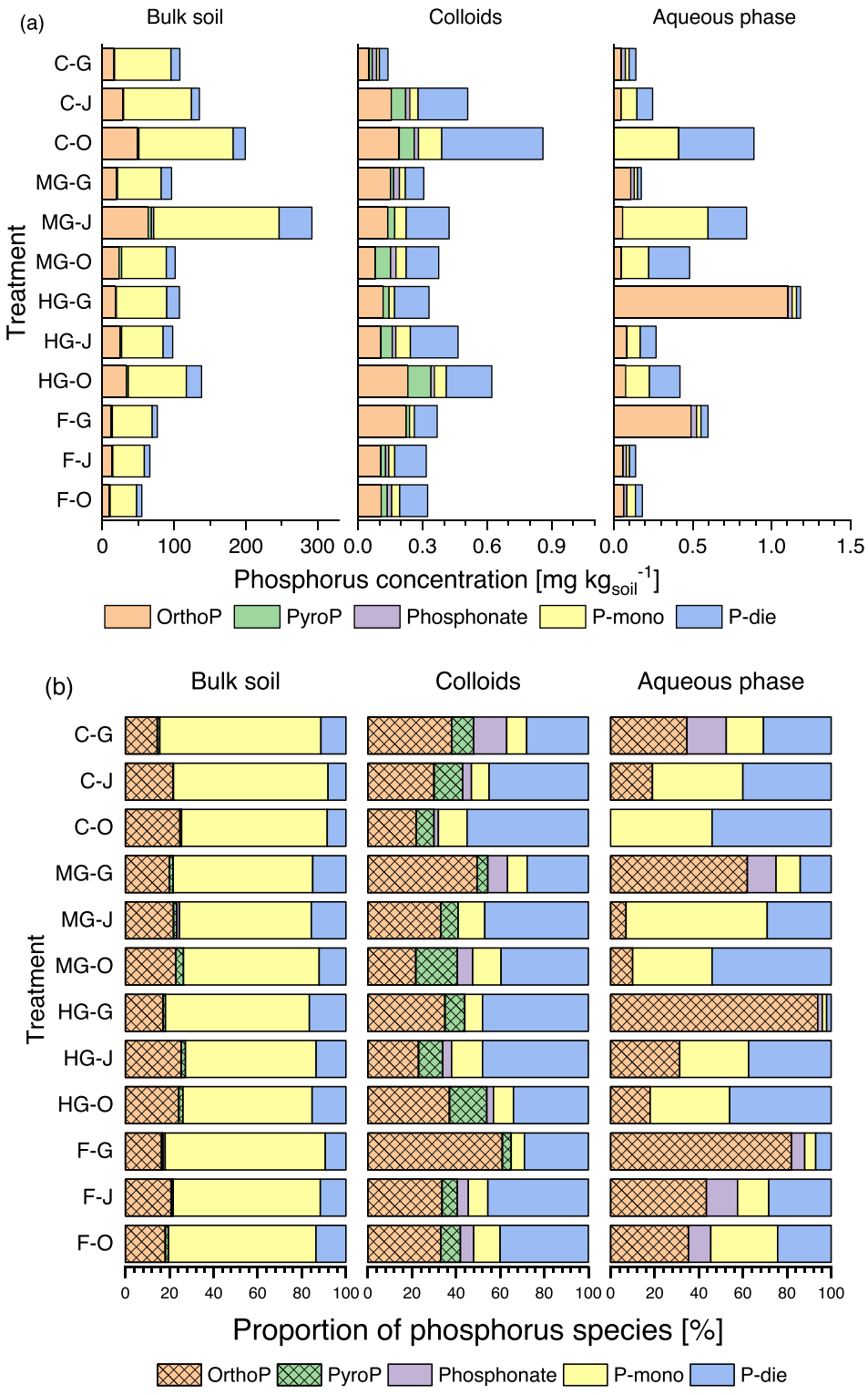

Fig. 5. Phosphorus composition and concentration (a) and percentages of each phosphorus species (b) in bulk soil (0–10 cm), 30–500 nm sized colloids and aqueous phase including nanocolloids < 30 nm. Treatments: C, Control; MG, Moderate Grazing; HG, Heavy Grazing; F, Fire. Vegetation types: G, Grassland; J, Juniper; O, Oak. It should be noted that the proportion of potential ribonucleic acid hydrolysis products was subtracted from the orthophosphate monoester (P-mono) proportion and was added to the orthophosphate diester (P-die) proportion.

(Fig. 2a), suggesting a balance between the output and input of elements like OC and P in this treatment, which differs from our third hypothesis that moderate grazing does stimulate colloid formation and related P retention. In contrast, heavy grazing significantly reduced WDC-OC in soils beneath oak (Fig. 2a). The potential excessive consumption of any grass under the heavy grazing beneath oak would reduce overall soil OC inputs and thus also decrease OC sequestration in WDC. Inputs from excreta may not offset the C removed by herbivore consumption in oak patches in the heavy grazing treatment since the animal excreta may be deposited on other portions of the landscape (Zhou et al., 2017), potentially facilitating the decrease of WDC-OC. Furthermore, the reduction in porosity caused by livestock trampling (Marquart et al., 2019) presumably impedes the vertical transport of mobile colloids and their interaction with soil, and may also induce OC and P loss through surface runoff (Chen and Arai, 2020). These results support our third hypothesis that colloid formation and related P retention are decreased by heavy grazing. Additional studies with increased sampling site density may help reveal in more detail how variations of different colloidal

sized soil fractions relate to their OC and nutrient content at a more regional scale.

The two grazing intensities did not differ with respect to either the mineral element concentrations of WDC (Fig. 2a), or the relative proportions of SOM, Ca, Mg and P in their three size fractions (Fig. 2b). In the soil beneath grass and juniper, both moderate and heavy grazing strengthen the association of Si, Al and Fe in fine colloids over medium colloids, compared to control (Fig. 2b), potentially implying the stabilization of colloidal clay minerals and/or Fe/Al-(hydr)oxides by OC. But when oak encroached, heavy grazing and less OC rearranged mineral elements in three size fractions (Fig. 2a), and favored the occurrence of clay and Fe/Al-(hydr)oxides colloids, resulting in greater abundance of medium sized colloids. This suggests a crucial effect of OC on clay and oxides distribution in colloids. Overall, the SOM enrichment due to woody encroachment favored especially the formation of smaller soil colloids in this savanna landscape, suggesting that woody encroachment has a greater effect on colloid formation than either grazing intensity or fire occurrence.

On oak encroached sites, both moderate and heavy grazing reduced P_o concentration in bulk soils, colloids and aqueous phase (Fig. 5). This could be attributable to higher rates of plant consumption by herbivores compared to rates of excreta inputs, resulting in a loss of total P_o from the soil. Furthermore, the ratio of P_i to P_o did not vary in bulk soil and colloids, indicating the balance between P_i consumption rate, P_o input and mineralization rate under grazing. But the ratio notably increased in the aqueous phase of grassland soils, implying grassland seepage maybe more sensitive to grazing. Further studies are needed to investigate the specific mechanisms of colloidal P_i to P_o balances under grazing intensities in savanna ecosystem.

4.4. Fire effect on WDC-elements

The influence of frequent fires exhibited diverse effects on elemental concentrations in whole soils and in colloidal soil fractions. The WDC-OC and -P concentrations were not affected significantly by fire on grass dominated portions of the landscape (Fig. 2a), perhaps due to relatively low rates of annual above- and belowground organic matter compared to woody patches. In soils beneath oak patches with higher OC and P concentrations (Table S1), fire markedly reduced their WDC concentrations compared to the control (Fig. 2a), perhaps due to the combustion of aboveground biomass and the litter layer (Mataix-Solera et al., 2011), and the enhanced loss rate of WDC through increased preferential flow paths in the burnt soil (Bian et al., 2019; Moody et al., 2013). This in part supported our third hypothesis that fire would weaken the colloid formation and related P retention, but only in oak encroached soil. The P loss rate may have been amplified through the elevated proportions of P_i dissolved in the "aqueous phase" of frequently burned sites (Fig. 5b). Merino et al. (2019) and Santin et al. (2018) demonstrated the appreciable shift of the extractable P from organic P to inorganic P probably due to mineralization with burning, which could accelerate P loss from soil.

However, fire did not significantly affect WDC-Ca, -Si, -Al, -Fe or -Mg concentrations in soils beneath any of the three vegetation types (Fig. 2a). These mineral elements are usually derived from the soil matrix, and our results suggest that fire amplifies their association in the larger medium-sized colloid fractions (Fig. 2b). Al/Fe (hydr)oxides could suffer dehydroxylation and aggregation into robust particles with higher aggregate stability after fire (Ulery et al., 2017; Yusiharni and Gilkes, 2012). Ulery et al. (1996) reported the thermal destruction of soil organic matter and phyllosilicates. The thermally altered soil organic matter and phyllosilicates might form medium-sized colloid aggregates. Mataix-Solera et al. (2011) reported increased soil aggregate stability with fire severity in soils with high clay and $CaCO_3$ concentrations, where Fe and Al oxides functioned as cementing agents. Our results revealed that fire can diminish the impact of woody encroachment on the WDC formation of savanna soil via thermal destruction and aggregation. More work is required to evaluate the behavior of colloidal P, OC and other soil elements in fire affected regions.

5. Conclusion

Woody encroachment increased colloidal OC, P and Ca concentrations and elevated their proportions in nanocolloid fractions (<30 nm), highlighting its potential mechanism via enhanced bulk SOM on soil nanocolloid formation in savanna ecosystems. Moderate grazing did not modify colloidal concentrations, while heavy grazing significantly reduced WDC-OC in oak encroached soil. Fire reduced colloidal OC and P concentrations and amplified the association of medium sized (160–500 nm) colloid fractions with Ca, Si, Al, Fe and Mg in nano- (<30 nm) and fine colloid (30–160 nm) fractions. Phosphorus was associated with Ca, Mg and Fe in the nanocolloid fraction (<30 nm) and to OC via Ca^{2+} bridging in fine and medium colloid (>30 nm) fractions. While bulk soils were dominated by monoester-P, the colloidal and "aqueous phase" containing < 30 nm colloids had more diester-P and inorganic P. Vegetation type was more important than grazing or fire as a determinant of soil colloidal size distribution and nutrient content in this savanna ecosystem. Our novel results on the behavior of soil colloids in response to long-term grazing, fire history, and woody plant encroachment provide mechanistic insights that will enhance our understanding of the influence of land cover and land use changes on the biogeochemistry of grasslands, savannas, and other dryland ecosystems.

Declaration of Competing Interest

The authors declare that they have no known competing financial interests or personal relationships that could have appeared to influence the work reported in this paper.

Data availability

No data was used for the research described in the article.

Acknowledgements

Qian Zhang would like to thank the China Scholarship Council (No. 201608420100) for supporting her study at RWTH Aachen University and Forschungszentrum Jülich. The authors would like to thank Dr. Sabine Willbold (ZEA-3, Forschungszentrum Jülich) for support with the ^{31}P-NMR measurements and Dr. Volker Nischwitz (ZEA-3, Forschungszentrum Jülich) for support with the ICP-MS measurements. Support was also provided by USDA/NIFA Hatch Project (1003961) and by the Texas A&M University Sid Kyle Global Savanna Research Initiative.

Note

The authors declare no competing financial interest.

Appendix A. Supplementary data

Supplementary data to this article can be found online at https://doi.org/10.1016/j.geoderma.2022.116282.

References

Ansley, R.J., Boutton, T.W., Skjemstad, J.O., 2006. Soil organic carbon and black carbon storage and dynamics under different fire regimes in temperate mixed-grass savanna. Glob. Biogeochem. Cycle 20 (3), 11.

Archer, S.R., Andersen, E.M., Predick, K.I., Schwinning, S., Steidl, R.J., Woods, S.R., 2017. Woody Plant Encroachment: Causes and Consequences. In: Briske, D.D. (Ed.), Rangeland Systems: Processes, Management and Challenges. Springer International Publishing, Cham, pp. 25–84.

Bendevis, M.A., Owens, M.K., Heilman, J.L., McInnes, K.J., 2010. Carbon exchange and water loss from two evergreen trees in a semiarid woodland. Ecohydrology 3 (1), 107–115.
Bian, F., Coleborn, K., Flemons, I., Baker, A., Treble, P.C., Hughes, C.E., Baker, A., Andersen, M.S., Tozer, M.G., Duan, W., Fogwill, C.J., Fairchild, I.J., 2019. Hydrological and geochemical responses of fire in a shallow cave system. Sci. Total Environ. 662, 180–191.
Blaser, W.J., Shanungu, G.K., Edwards, P.J., Venterink, H.O., 2014. Woody encroachment reduces nutrient limitation and promotes soil carbon sequestration. Ecol. Evol. 4 (8), 1423–1438.
Boutton, T.W., Archer, S.R., Midwood, A.J., Zitzer, S.F., Bol, R., 1998. $\delta^{13}C$ values of soil organic carbon and their use in documenting vegetation change in a subtropical savanna ecosystem. Geoderma 82 (1), 5–41.
Buitenwerf, R., Bond, W.J., Stevens, N., Trollope, W.S.W., 2012. Increased tree densities in South African savannas: > 50 years of data suggests CO_2 as a driver. Glob. Change Biol. 18 (2), 675–684.
Byrnes, R.C., Eastburn, D.J., Tate, K.W., Roche, L.M., 2018. A global meta-analysis of grazing impacts on soil health indicators. J. Environ. Qual. 47 (4), 758–765.
Cade-Menun, B.J., 2015. Improved peak identification in ^{31}P-NMR spectra of environmental samples with a standardized method and peak library. Geoderma 257–258, 102–114.
Cade-Menun, B., Preston, C., 1996. A comparison of soil extraction procedures for 31P NMR spectroscopy. Soil Sci. 161 (11), 770–785.
Chen, A., Arai, Y., 2020. Current uncertainties in assessing the colloidal phosphorus loss from soil. In: Sparks, D.L. (Ed.), Advances in Agronomy. Academic Press, pp. 117–151.
Coetsee, C., Bond, W.J., February, E.C., 2010. Frequent fire affects soil nitrogen and carbon in an African savanna by changing woody cover. Oecologia 162 (4), 1027–1034.
Dlamini, P., Mbanjwa, V., Gxasheka, M., Tyasi, L., Sekhohola-Dlamini, L., 2019. Chemical stabilisation of carbon stocks by polyvalent cations in plinthic soil of a shrub-encroached savanna grassland, South Africa. Catena 181, 10.
Eldridge, D.J., Bowker, M.A., Maestre, F.T., Roger, E., Reynolds, J.F., Whitford, W.G., 2011. Impacts of shrub encroachment on ecosystem structure and functioning: Towards a global synthesis. Ecol. Lett. 14 (7), 709–722.
Eldridge, D.J., Delgado-Baquerizo, M., Travers, S.K., Val, J., Oliver, I., Hamonts, K., Singh, B.K., 2017. Competition drives the response of soil microbial diversity to increased grazing by vertebrate herbivores. Ecology 98 (7), 1922–1931.
Farella, M.M., Breshears, D.D., Gallery, R.E., 2020. Predicting drivers of collective soil function with woody plant encroachment in complex landscapes. J. Geophys. Res.-Biogeosci. 125 (12), 17.
Fuhlendorf, S.D., Smeins, F.E., 1997. Long-term vegetation dynamics mediated by herbivores, weather and fire in a *Juniperus-Quercus* savanna. J. Veg. Sci. 8 (6), 819–828.
George, T.S., Giles, C.D., Menezes-Blackburn, D., Condron, L.M., Gama-Rodrigues, A.C., Jaisi, D., Lang, F., Neal, A.L., Stutter, M.I., Almeida, D.S., Bol, R., Cabugao, K.G., Celi, L., Cotner, J.B., Feng, G., Goll, D.S., Hallama, M., Krueger, J., Plassard, C., Rosling, A., Darch, T., Fraser, T., Giesler, R., Richardson, A.E., Tamburini, F., Shand, C.A., Lumsdon, D.G., Zhang, H., Blackwell, M.S.A., Wearing, C., Mezeli, M. M., Almas, A.R., Audette, Y., Bertrand, I., Beyhaut, E., Boitt, G., Bradshaw, N., Brearley, C.A., Bruulsema, T.W., Ciais, P., Cozzolino, V., Duran, P.C., Mora, M.L., de Menezes, A.B., Dodd, R.J., Dunfield, K., Engl, C., Frazao, J.J., Garland, G., Jimenez, J.L.G., Graca, J., Granger, S.J., Harrison, A.F., Heuck, C., Hou, E.Q., Johnes, P.J., Kaiser, K., Kjaer, H.A., Klumpp, E., Lamb, A.L., Macintosh, K.A., Mackay, E.B., McGrath, J., McIntyre, C., McLaren, T., Meszaros, E., Missong, A., Mooshammer, M., Negron, C.P., Nelson, L.A., Pfahler, V., Poblete-Grant, P., Randall, M., Seguel, A., Seth, K., Smith, A.C., Smits, M.M., Sobarzo, J.A., Spohn, M., Tawaraya, K., Tibbett, M., Voroney, P., Wallander, H., Wang, L., Wasaki, J., Haygarth, P.M., 2018. Organic phosphorus in the terrestrial environment: A perspective on the state of the art and future priorities (vol 427, pg 191, 2018). Plant Soil 427 (1–2), 209–211.
Giddings, J.C., 1993. Field-flow fractionation: Analysis of macromolecular, colloidal, and particulate materials. Science 260 (5113), 1456–1465.
Gottselig, N., Nischwitz, V., Meyn, T., Amelung, W., Bol, R., Halle, C., Vereecken, H., Siemens, J., Klumpp, E., 2017. Phosphorus binding to nanoparticles and colloids in forest stream waters. Vadose Zone J. 16 (3), 12.
Guggenberger, G., Haider, K.M., 2001. Effect of mineral colloids on biogeochemical cycling of C, N, P, and S in soil. In: Huang, P.M., Bollag, J.M., Senesi, N. (Eds.), Interactions Between Soil Particles and Microorganisms: Impact on the Terrestrial Ecosystem. John Wiley & Sons Ltd, Chichester, UK, pp. 267–322.
Hathaway, J.C., 1956. Procedure for clay mineral analyses used in the sedimentary petrology laboratory of the U.S. Geological Survey. Clay Minerals Bulletin 3(15), 8-13.
Hatten, J.A., Zabowski, D., 2009. Changes in soil organic matter pools and carbon mineralization as influenced by fire severity. Soil Sci. Soc. Am. J. 73 (1), 262–273.
He, M., Zhou, G., Yuan, T., van Groenigen, K.J., Shao, J., Zhou, X., 2020. Grazing intensity significantly changes the C:N: P stoichiometry in grassland ecosystems. Glob. Ecol. Biogeogr. 29 (2), 355–369.
Henderson, R., Kabengi, N., Mantripragada, N., Cabrera, M., Hassan, S., Thompson, A., 2012. Anoxia-induced release of colloid- and nanoparticle-bound phosphorus in grassland soils. Environ. Sci. Technol. 46 (21), 11727–11734.
Holdo, R.M., Mack, M.C., Arnold, S.G., 2012. Tree canopies explain fire effects on soil nitrogen, phosphorus and carbon in a savanna ecosystem. J. Veg. Sci. 23 (2), 352–360.
Holdo, R.M., Onderdonk, D.A., Barr, A.G., Mwita, M., Anderson, T.M., 2020. Spatial transitions in tree cover are associated with soil hydrology, but not with grass biomass, fire frequency, or herbivore biomass in Serengeti savannahs. J. Ecol. 108 (2), 586–597.
Holzmann, S., Missong, A., Puhlmann, H., Siemens, J., Bol, R., Klumpp, E., Wilpert, K.v., 2016. Impact of anthropogenic induced nitrogen input and liming on phosphorus leaching in forest soils. J. Plant Nutr. Soil Sci. 179 (4), 443–453.
Houghton, R.A., 2014. The Contemporary Carbon Cycle. In: Holland, H.D., Turekian, K. K. (Eds.), Treatise on Geochemistry, Second Edition. Elsevier, Oxford, pp. 399–435.
Javidpour, J., Molinero, J.C., Lehmann, A., Hansen, T., Sommer, U., 2009. Annual assessment of the predation of *Mnemiopsis leidyi* in a new invaded environment, the Kiel Fjord (Western Baltic Sea): A matter of concern? J. Plankton Res. 31 (7), 729–738.
Jessup, K.E., Barnes, P.W., Boutton, T.W., 2003. Vegetation dynamics in a *Quercus-Juniperus* savanna: An isotopic assessment. J. Veg. Sci. 14 (6), 841–852.
Jiang, X., Bol, R., Willbold, S., Vereecken, H., Klumpp, E., 2015. Speciation and distribution of P associated with Fe and Al oxides in aggregate-sized fraction of an arable soil. Biogeosciences 12 (21), 6443–6452.
Jiang, X.Q., Bol, R., Cade-Menun, B.J., Nischwitz, V., Willbold, S., Bauke, S.L., Vereecken, H., Amelung, W., Klumpp, E., 2017. Colloid-bound and dissolved phosphorus species in topsoil water extracts along a grassland transect from Cambisol to Stagnosol. Biogeosciences 14 (5), 1153–1164.
Konrad, A., Billiy, B., Regenbogen, P., Bol, R., Lang, F., Klumpp, E., Siemens, J., 2021. Forest soil colloids enhance delivery of phosphorus into a Diffusive Gradient in Thin films (DGT) sink. Front. For. Glob. Change 3 (158), 11.
Krause, L., Rodionov, A., Schweizer, S.A., Siebers, N., Lehndorff, E., Klumpp, E., Amelung, W., 2018. Microaggregate stability and storage of organic carbon is affected by clay content in arable Luvisols. Soil Tillage Res. 182, 123–129.
Krause, L., Klumpp, E., Nofz, I., Missong, A., Amelung, W., Siebers, N., 2020. Colloidal iron and organic carbon control soil aggregate formation and stability in arable Luvisols. Geoderma 374, 114421.
Krull, E.S., Skjemstad, J.O., Burrows, W.H., Bray, S.G., Wynn, J.G., Bol, R., Spouncer, L., Harms, B., 2005. Recent vegetation changes in central Queensland, Australia: Evidence from δ13C and 14C analyses of soil organic matter. Geoderma 126 (3), 241–259.
Lang, F., Bauhus, J., Frossard, E., George, E., Kaiser, K., Kaupenjohann, M., Kruger, J., Matzner, E., Polle, A., Prietzel, J., Rennenberg, H., Wellbrock, N., 2016. Phosphorus in forest ecosystems: New insights from an ecosystem nutrition perspective. J. Plant Nutr. Soil Sci. 179 (2), 129–135.
Lehmann, C.E.R., Archibald, S.A., Hoffmann, W.A., Bond, W.J., 2011. Deciphering the distribution of the savanna biome. New Phytol. 191 (1), 197–209.
Leitner, M., Davies, A.B., Parr, C.L., Eggleton, P., Robertson, M.P., 2018. Woody encroachment slows decomposition and termite activity in an African savanna. Glob. Change Biol. 24 (6), 2597–2606.
Lekfeldt, J.D.S., Kjaergaard, C., Magid, J., 2017. Long-term Effects of Organic Waste Fertilizers on Soil Structure, Tracer Transport, and Leaching of Colloids. J. Environ. Qual. 46 (4), 862–870.
Li, F.Y., Liang, X.Q., Liu, Z.W., Tian, G.M., 2019. No-till with straw return retains soil total P while reducing loss potential of soil colloidal P in rice-fallow systems. Agric. Ecosyst. Environ. 286, 106653.
Li, D.J., Wen, L., Yang, L.Q., Luo, P., Xiao, K.C., Chen, H., Zhang, W., He, X.Y., Chen, H. S., Wang, K.L., 2017. Dynamics of soil organic carbon and nitrogen following agricultural abandonment in a karst region. J. Geophys. Res.-Biogeosci. 122 (1), 230–242.
Li, F.Y., Zhang, Q., Klumpp, E., Bol, R., Nischwitz, V., Ge, Z., Liang, X.Q., 2021. Organic carbon linkage with soil colloidal phosphorus at regional and field scales: Insights from size fractionation of fine particles. Environ. Sci. Technol. 55 (9), 5815–5825.
Liang, M., Smith, N.G., Chen, J., Wu, Y., Guo, Z., Gornish, E.S., Liang, C., 2021. Shifts in plant composition mediate grazing effects on carbon cycling in grasslands. J. Appl. Ecol. 58 (3), 518–527.
Liao, J.D., Boutton, T.W., 2008. Soil microbial biomass response to woody plant invasion of grassland. Soil Biol. Biochem. 40 (5), 1207–1216.
Liao, J.D., Boutton, T.W., Jastrow, J.D., 2006. Storage and dynamics of carbon and nitrogen in soil physical fractions following woody plant invasion of grassland. Soil Biol. Biochem. 38 (11), 3184–3196.
Marquart, A., Eldridge, D.J., Travers, S.K., Val, J., Blaum, N., 2019. Large shrubs partly compensate negative effects of grazing on hydrological function in a semi-arid savanna. Basic Appl. Ecol. 38, 58–68.
Marshall, S.B., 1995. Biogeochemical Consequences of Livestock Grazing in a Juniper-oak Savanna. Texas A&M University.
Mataix-Solera, J., Cerda, A., Arcenegui, V., Jordan, A., Zavala, L.M., 2011. Fire effects on soil aggregation: A review. Earth-Sci. Rev. 109 (1–2), 44–60.
McCulley, R.L., Archer, S.R., Boutton, T.W., Hons, F.M., Zuberer, D.A., 2004. Soil respiration and nutrient cycling in wooded communities developing in grassland. Ecology 85 (10), 2804–2817.
McSherry, M.E., Ritchie, M.E., 2013. Effects of grazing on grassland soil carbon: A global review. Glob. Change Biol. 19 (5), 1347–1357.
Menezes-Blackburn, D., Bol, R., Klumpp, E., Missong, A., Nischwitz, V., Haygarth, P.M., 2021. Citric acid effect on the abundance, size and composition of water-dispersible soil colloids and its relationship to soil phosphorus desorption: A case study. J. Soil Sci. Plant Nutr. 21 (3), 2436–2446.
Merino, A., Jimenez, E., Fernandez, C., Fonturbel, M.T., Campo, J., Vega, J.A., 2019. Soil organic matter and phosphorus dynamics after low intensity prescribed burning in forests and shrubland. J. Environ. Manage. 234, 214–225.
Milchunas, D.G., Lauenroth, W.K., 1993. Quantitative effects of grazing on vegetation and soils over a global range of environments. Ecol. Monogr. 63 (4), 327–366.

Mills, T.J., Anderson, S.P., Bern, C., Aguirre, A., Derry, L.A., 2017. Colloid mobilization and seasonal variability in a semiarid headwater stream. J. Environ. Qual. 46 (1), 88–95.
Missong, A., Bol, R., Willbold, S., Siemens, J., Klumpp, E., 2016. Phosphorus forms in forest soil colloids as revealed by liquid-state ^{31}P-NMR. J. Plant Nutr. Soil Sci. 179 (2), 159–167.
Missong, A., Bol, R., Nischwitz, V., Krüger, J., Lang, F., Siemens, J., Klumpp, E., 2018a. Phosphorus in water dispersible-colloids of forest soil profiles. Plant Soil 427 (1), 71–86.
Missong, A., Holzmann, S., Bol, R., Nischwitz, V., Puhlmann, H., von Wilpert, K., Siemens, J., Klumpp, E., 2018b. Leaching of natural colloids from forest topsoils and their relevance for phosphorus mobility. Sci. Total Environ. 634, 305–315.
Moody, J.A., Shakesby, R.A., Robichaud, P.R., Cannon, S.H., Martin, D.A., 2013. Current research issues related to post-wildfire runoff and erosion processes. Earth-Sci. Rev. 122, 10–37.
Moradi, G., Bol, R., Trbojevic, L., Missong, A., Mörchen, R., Fuentes, B., May, S.M., Lehndorff, E., Klumpp, E., 2020. Contrasting depth distribution of colloid-associated phosphorus in the active and abandoned sections of an alluvial fan in a hyper-arid region of the Atacama Desert. Glob. Planet. Change 185, 103090.
O'Brien, S.L., Jastrow, J.D., Grimley, D.A., Gonzalez-Meler, M.A., 2015. Edaphic controls on soil organic carbon stocks in restored grasslands. Geoderma 251–252, 117–123.
Pang, L., Lafogler, M., Knorr, B., McGill, E., Saunders, D., Baumann, T., Abraham, P., Close, M., 2016. Influence of colloids on the attenuation and transport of phosphorus in alluvial gravel aquifer and vadose zone media. Sci. Total Environ. 550, 60–68.
Pellegrini, A.F.A., Hedin, L.O., Staver, A.C., Govender, N., 2015. Fire alters ecosystem carbon and nutrients but not plant nutrient stoichiometry or composition in tropical savanna. Ecology 96 (5), 1275–1285.
Pellegrini, A.F.A., Ahlström, A., Hobbie, S.E., Reich, P.B., Nieradzik, L.P., Staver, A.C., Scharenbroch, B.C., Jumpponen, A., Anderegg, W.R.L., Randerson, J.T., Jackson, R. B., 2018. Fire frequency drives decadal changes in soil carbon and nitrogen and ecosystem productivity. Nature 553 (7687), 194–198.
Pellegrini, A.F.A., McLauchlan, K.K., Hobbie, S.E., Mack, M.C., Marcotte, A.L., Nelson, D. M., Perakis, S.S., Reich, P.B., Whittinghill, K., 2020. Frequent burning causes large losses of carbon from deep soil layers in a temperate savanna. J. Ecol. 108 (4), 1426–1441.
Pineiro, G., Paruelo, J.M., Jobbagy, E.G., Jackson, R.B., Oesterheld, M., 2009. Grazing effects on belowground C and N stocks along a network of cattle exclosures in temperate and subtropical grasslands of South America. Glob. Biogeochem. Cycle 23, 14.
Rodrigues, M., Pavinato, P.S., Withers, P.J.A., Teles, A.P.B., Herrera, W.F.B., 2016. Legacy phosphorus and no tillage agriculture in tropical oxisols of the Brazilian savanna. Sci. Total Environ. 542, 1050–1061.
Rossatto, D.R., Rigobelo, E.C., 2016. Tree encroachment into savannas alters soil microbiological and chemical properties facilitating forest expansion. J. For. Res. 27 (5), 1047–1054.
Rowley, M.C., Grand, S., Verrecchia, E.P., 2018. Calcium-mediated stabilisation of soil organic carbon. Biogeochemistry 137 (1–2), 27–49.
Rowley, M.C., Grand, S., Spangenberg, J.E., Verrecchia, E.P., 2021. Evidence linking calcium to increased organo-mineral association in soils. Biogeochemistry 153 (3), 223–241.
Sanderson, J.S., Beutler, C., Brown, J.R., Burke, I., Chapman, T., Conant, R.T., Derner, J. D., Easter, M., Fuhlendorf, S.D., Grissom, G., Herrick, J.E., Liptzin, D., Morgan, J.A., Murph, R., Pague, C., Rangwala, I., Ray, D., Rondeau, R., Schulz, T., Sullivan, T., 2020. Cattle, conservation, and carbon in the western Great Plains. J. Soil Water Conserv. 75 (1), 5A–12A.
Sankaran, M., Hanan, N.P., Scholes, R.J., Ratnam, J., Augustine, D.J., Cade, B.S., Gignoux, J., Higgins, S.I., Le Roux, X., Ludwig, F., Ardo, J., Banyikwa, F., Bronn, A., Bucini, G., Caylor, K.K., Coughenour, M.B., Diouf, A., Ekaya, W., Feral, C.J., February, E.C., Frost, P.G.H., Hiernaux, P., Hrabar, H., Metzger, K.L., Prins, H.H.T., Ringrose, S., Sea, W., Tews, J., Worden, J., Zambatis, N., 2005. Determinants of woody cover in African savannas. Nature 438 (7069), 846–849.
Santin, C., Otero, X.L., Doerr, S.H., Chafer, C.J., 2018. Impact of a moderate/high-severity prescribed eucalypt forest fire on soil phosphorous stocks and partitioning. Sci. Total Environ. 621, 1103–1114.
Schimpf, M.E., Caldwell, K., Giddings, J.C., 2000. Field-flow Fractionation Handbook. John Wiley & Sons.
Schwertmann, U., Fechter, H., 1982. The point of zero charge of natural and synthetic ferrihydrites and its relation to adsorbed silicate. Clay Min. 17 (4), 471–476.
Séquaris, J.M., Lewandowski, H., 2003. Physicochemical characterization of potential colloids from agricultural topsoils. Colloids Surf. A Physicochem. Eng. Asp. 217 (1), 93–99.
Seta, A.K., Karathanasis, A.D., 1996. Water dispersible colloids and factors influencing their dispersibility from soil aggregates. Geoderma 74 (3), 255–266.
Siemens, J., Ilg, K., Pagel, H., Kaupenjohann, M., 2008. Is colloid-facilitated phosphorus leaching triggered by phosphorus accumulation in sandy soils? J. Environ. Qual. 37 (6), 2100–2107.
Sitters, J., Edwards, P.J., Venterink, H.O., 2013. Increases of soil C, N, and P pools along an Acacia tree density gradient and their effects on trees and grasses. Ecosystems 16 (2), 347–357.
Sitters, J., Kimuyu, D.M., Young, T.P., Claeys, P., Olde Venterink, H., 2020. Negative effects of cattle on soil carbon and nutrient pools reversed by megaherbivores. Nat. Sustain. 3 (5), 360–366.
Smeins, F.E., Taylor, T.W., Merrill, L.B., 1976. Vegetation of a 25-year exclosure on the Edwards Plateau, Texas. Soc. Range Manage. 24–29.
Smernik, R.J., Doolette, A.L., Noack, S.R., 2015. Identification of RNA hydrolysis products in NaOH-EDTA extracts using ^{31}P NMR spectroscopy. Commun. Soil Sci. Plant Anal. 46 (21), 2746–2756.
Somasundaran, P., Agar, G.E., 1967. The zero point of charge of calcite. J. Colloid Interface Sci. 24 (4), 433–440.
Stevens, N., Lehmann, C.E.R., Murphy, B.P., Durigan, G., 2017. Savanna woody encroachment is widespread across three continents. Glob. Change Biol. 23 (1), 235–244.
Sun, Y., Pan, D., Wei, X., Xian, D., Wang, P., Hou, J., Xu, Z., Liu, C., Wu, W., 2020. Insight into the stability and correlated transport of kaolinite colloid: Effect of pH, electrolytes and humic substances. Environ. Pollut. 266, 115189.
Taylor, C.A., Twidwell, D.r.c., Garza, N.E., Rosser, C.l.n., Hoffman, J.K., Brooks, T.D., 2012. Long-term effects of fire, livestock herbivory removal, and weather variability in Texas semiarid savanna. Rangel. Ecol. Manag. 65 (1), 21–30.
Tsiantos, C., Gionis, V., Chryssikos, G.D., 2018. Smectite in bentonite: Near infrared systematics and estimation of layer charge. Appl. Clay Sci. 160, 81–87.
Turner, B.L., Kay, M.A., Westermann, D.T., 2004. Colloidal phosphorus in surface runoff and water extracts from semiarid soils of the western United States. J. Environ. Qual. 33 (4), 1464–1472.
Turner, B.L., Brenes-Arguedas, T., Condit, R., 2018. Pervasive phosphorus limitation of tree species but not communities in tropical forests. Nature 555 (7696), 367–370.
Ulery, A.L., Graham, R.C., Bowen, L.H., 1996. Forest fire effects on soil phyllosilicates in California. Soil Sci. Soc. Am. J. 60 (1), 309–315.
Ulery, A.L., Graham, R.C., Goforth, B.R., Hubbert, K.R., 2017. Fire effects on cation exchange capacity of California forest and woodland soils. Geoderma 286, 125–130.
USDA/NRCS, 2015. Custom Soil Resources Report for Edwards and Real Counties, and Sutton County. Texas, USDA Natural Resource Conservation Service, Washington, D. C.
Wang, L., Missong, A., Amelung, W., Willbold, S., Prietzel, J., Klumpp, E., 2020. Dissolved and colloidal phosphorus affect P cycling in calcareous forest soils. Geoderma 375, 114507.
Yan, J., Manelski, R., Vasilas, B., Jin, Y., 2018. Mobile colloidal organic carbon: An underestimated carbon pool in global carbon cycles? Front. Environ. Sci. 6, 12.
Yu, B.Q., Xie, C.K., Cai, S.Z., Chen, Y., Lv, Y.P., Mo, Z.L., Liu, T.L., Yang, Z.W., 2018. Effects of tree root density on soil total porosity and non-capillary porosity using a ground-penetrating tree radar unit in Shanghai. China. Sustain. 10 (12), 4640.
Yusiharni, E., Gilkes, R.J., 2012. Changes in the mineralogy and chemistry of a lateritic soil due to a bushfire at Wundowie, Darling Range, Western Australia. Geoderma 191, 140–150.
Zhang, Q., Bol, R., Amelung, W., Missong, A., Siemens, J., Mulder, I., Willbold, S., Muller, C., Muniz, A.W., Klumpp, E., 2021. Water dispersible colloids and related nutrient availability in Amazonian Terra Preta soils. Geoderma 397, 11.
Zhao, H.M., Tong, D.Q., Lin, Q.X., Lu, X.G., Wang, G.P., 2012. Effect of fires on soil organic carbon pool and mineralization in a Northeastern China wetland. Geoderma 189, 532–539.
Zhou, Y., Boutton, T.W., Wu, X.B., 2018. Woody plant encroachment amplifies spatial heterogeneity of soil phosphorus to considerable depth. Ecology 99 (1), 136–147.
Zhou, G.Y., Zhou, X.H., He, Y.H., Shao, J.J., Hu, Z.H., Liu, R.Q., Zhou, H.M., Hosseinibai, S., 2017. Grazing intensity significantly affects belowground carbon and nitrogen cycling in grassland ecosystems: A meta-analysis. Glob. Change Biol. 23 (3), 1167–1179.

Supplementary Information

Soil colloidal particles in a subtropical savanna: Biogeochemical significance and influence of anthropogenic disturbances

Qian Zhang[1,2], Thomas W. Boutton[3], Che-Jen Hsiao[3], Ryan M. Mushinski[3,4], Liming Wang[1], Roland Bol[1,5], Erwin Klumpp[1]

1. Institute of Bio- and Geosciences, Agrosphere (IBG-3), Forschungszentrum Jülich, Wilhelm-Johnen-Str., 52425 Jülich, Germany

2. Institute for Environmental Research (Biology V), RWTH Aachen University, 52074 Aachen, Germany

3. Department of Ecology and Conservation Biology, Texas A&M University, College Station, TX 77843, USA

4. School of Life Sciences, University of Warwick, Coventry, CV4 7AL, UK

5. School of Natural Sciences, Environment Centre Wales, Bangor University, Bangor, LL57 2UW, UK

Corresponding author: zhangqian90@foxmail.com

Section S1: Calculation of centrifugation time

Table S1. Soil properties by treatment and vegetation type.

Table S2. Parameters and conditions for asymmetric flow field-flow fractionation separation.

Figure S1. Mass percentages of water extractable phase (WEP) (including the < 500 nm water dispersible colloids and solutes) in studied soils.

Figure S2. Field-flow fractionation-ICP-MS fractograms (Si, Fe, Mg and UV signals) of water-dispersible colloids from 12 soil sites with different treatments.

Figure S3. Concentrations of P, OC, Ca, Mg, Al, Fe and Si (mg kg_{soil}^{-1}) in water dispersible colloids (< 500 nm) and three size fraction colloids.

Figure S4. ^{13}P-nuclear magnetic resonance (NMR) spectra of bulk soils, colloids (30-500 nm) and aqueous phase including colloids < 30 nm.

Section S1: Calculation of centrifugation time

The mixture of soil and Milli-Q water was settled for a while and when centrifuged to obtain the water-dispersible colloids. Sedimentation time was calculated for the desired particle size by Stoke's law.

- Equation for calculation of sedimentation velocity (v):

$$v = \frac{2}{9}\frac{(\rho_p - \rho_f)}{\mu} g R^2$$

where

v is the velocity (m s^{-1});

ρ_p is the mass density of the particles (2.0 g cm^{-3} for > 2 µm particles);

ρ_f is the mass density of water (1.0 g cm^{-3});

μ is the dynamic viscosity of water (1.0016 g m^{-1} s^{-1}) at 20 °C;

g is the gravitational acceleration (9.81 m s^{-2});

R is the radius of the target particle.

- Equation for calculation of the precipitation time (t):

$$t = \frac{H}{v}$$

where H is the depth of the suspension.

Following sedimentation, the non-settling supernatant phase was centrifuged to obtain the desired colloids. Centrifugation was carried out with a Beckman Coulter Avanti J Centrifuge equipped with a JA14 fixed angle (25°) rotor. The centrifugation time was calculated as below.

- Equation for calculation of the centrifugation time (T):

$$T = \frac{\eta \, log_{10}\left(\frac{R_2}{R_1}\right)}{3.81 \, r^2 N^2 \left(\rho_p - \rho_0\right)} + \frac{2(t_a + t_d)}{3}$$

where

T is the total time (s);

η is the dynamic viscosity of water (1.0016 g m^{-1} s^{-1}) at 20 °C;

R_1 is the initial distance of the particle from axis of rotation (cm);

R_2 is the final distance of the particle from axis of rotation (cm);

r is the radius of the particle (cm);

N is the angular velocity (111.46 rad s^{-1});

ρ_p is the density of the particle (1.5 g cm^{-3});

ρ_0 is the density of the medium (1.0 g cm^{-3} for water);

t_a is the time of acceleration of the centrifuge (20 s);

t_d is the time of deceleration of the centrifuge (20 s).

Table S1. Soil properties by treatment and vegetation type at the Texas A&M AgriLife Sonora Research Station. Treatments and vegetation types are described in the Methods section. Values are means and standard deviations (N = 3 for each treatment combination). SOC = soil organic carbon, TN = total nitrogen, and TP = total phosphorus.

Treatment	Vegetation	pH	Sand (%)	Silt (%)	Clay (%)	SOC (%)	TN (%)	TP (%)
Control	Grass	7.69 (0.02)	11.4 (1.2)	43.7 (1.3)	44.9 (2.1)	4.6 (0.3)	0.45 (0.02)	0.066 (0.001)
	Juniper	7.56 (0.03)	17.5 (4.6)	42.2 (2.7)	40.3 (6.3)	8.9 (1.7)	0.62 (0.11)	0.075 (0.017)
	Oak	7.63 (0.02)	24.5 (2.3)	40.0 (0.4)	34.5 (2.7)	13.6 (2.2)	1.02 (0.17)	0.110 (0.011)
Moderate grazing	Grass	7.57 (0.04)	10.0 (3.1)	36.0 (5.2)	54.0 (5.2)	4.5 (0.2)	0.43 (0.03)	0.062 (0.006)
	Juniper	7.61 (0.10)	15.4 (1.6)	41.4 (2.4)	43.2 (1.9)	9.6 (1.3)	0.70 (0.11)	0.079 (0.014)
	Oak	7.61 (0.05)	21.0 (4.6)	35.2 (3.1)	43.8 (7.7)	10.2 (0.2)	0.77 (0.02)	0.075 (0.016)
Heavy grazing	Grass	7.59 (0.03)	16.7 (2.3)	38.3 (1.5)	45.0 (3.1)	3.8 (0.3)	0.38 (0.02)	0.058 (0.004)
	Juniper	7.61 (0.04)	22.9 (2.1)	34.1 (1.1)	43.0 (2.1)	8.3 (1.4)	0.58 (0.06)	0.056 (0.003)
	Oak	7.54 (0.02)	17.5 (5.7)	38.1 (6.9)	44.4 (1.6)	8.1 (1.3)	0.65 (0.08)	0.072 (0.006)
Fire	Grass	7.79 (0.06)	8.4 (0.6)	40.9 (2.3)	50.7 (2.2)	3.4 (0.6)	0.34 (0.05)	0.060 (0.001)
	Juniper	7.60 (0.09)	11.7 (3.6)	42.8 (3.0)	45.6 (4.3)	4.2 (0.6)	0.40 (0.04)	0.063 (0.008)
	Oak	7.58 (0.04)	13.9 (2.0)	35.0 (1.0)	51.1 (2.6)	5.5 (0.7)	0.49 (0.06)	0.074 (0.005)

Table S2. Parameters and conditions for asymmetric flow field-flow fractionation separation.

Parameter	
Membrane	PES (1 kDa)
Spacer	350 µm
Carrier solution	25 µM NaCl in deionised water
Detector flow	0.5 mL min^{-1}
Injection volume	4000 µL
Injection flow	0.3 mL min^{-1}
Injection time	25 min
Method	
Cross-flow1	2.5 mL min^{-1}
t0 - t1 Focus time	25 min
t1 - t2 Transition time	1 min
t3 – t4 Constant flow	0.5 min
t4 – t5 Power mode (0.2 exponential)	20 min
Cross-flow2	0.15 mL min^{-1}
t5 – t6 Power mode (0.8 exponential)	10 min
Cross-flow3	0 mL min^{-1}
t5 – t6 Constant flow	60 min

Figure S1. Mass percentages of water extractable phase (WEP) (including the < 500 nm water dispersible colloids and solutes) in studied soils. Lowercases represent difference between vegetation type ($p < 0.05$).

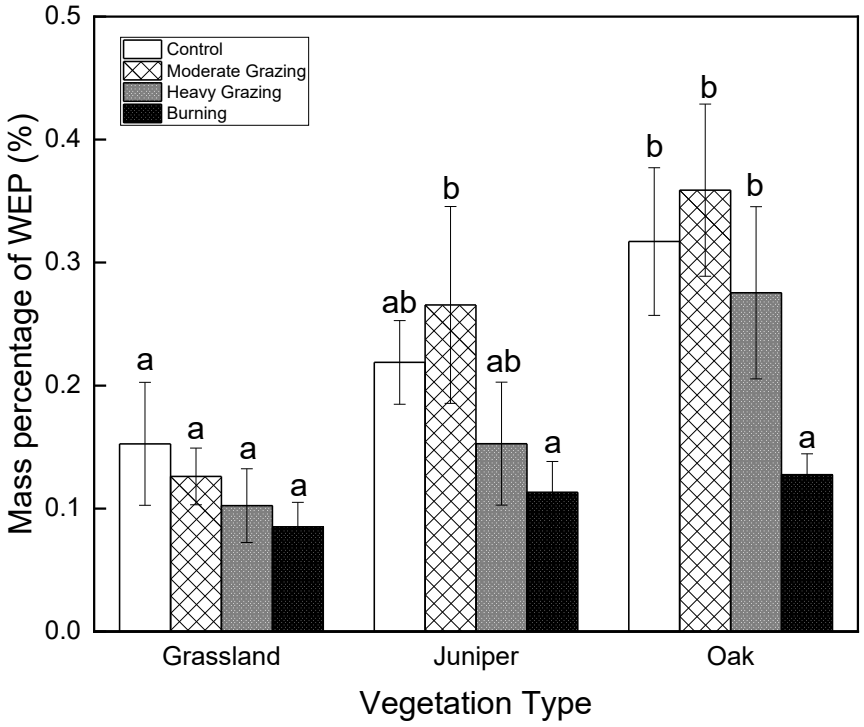

Figure S2. Field-flow fractionation-ICP-MS fractograms (Si, Fe, Mg and UV signals) of water-dispersible colloids from 12 soil sites with different treatments. The concentration ($\mu g\ kg_{soil}^{-1}$) of each element in the y-axis was converted from OCD and ICP-MS signals, respectively. The elution time scale (min) in the x-axis is related to particle size. C=Control; F=Fire; MG= Moderate Grazing; HG= Heavy Grazing. One from every three replicates was selected for the figures.

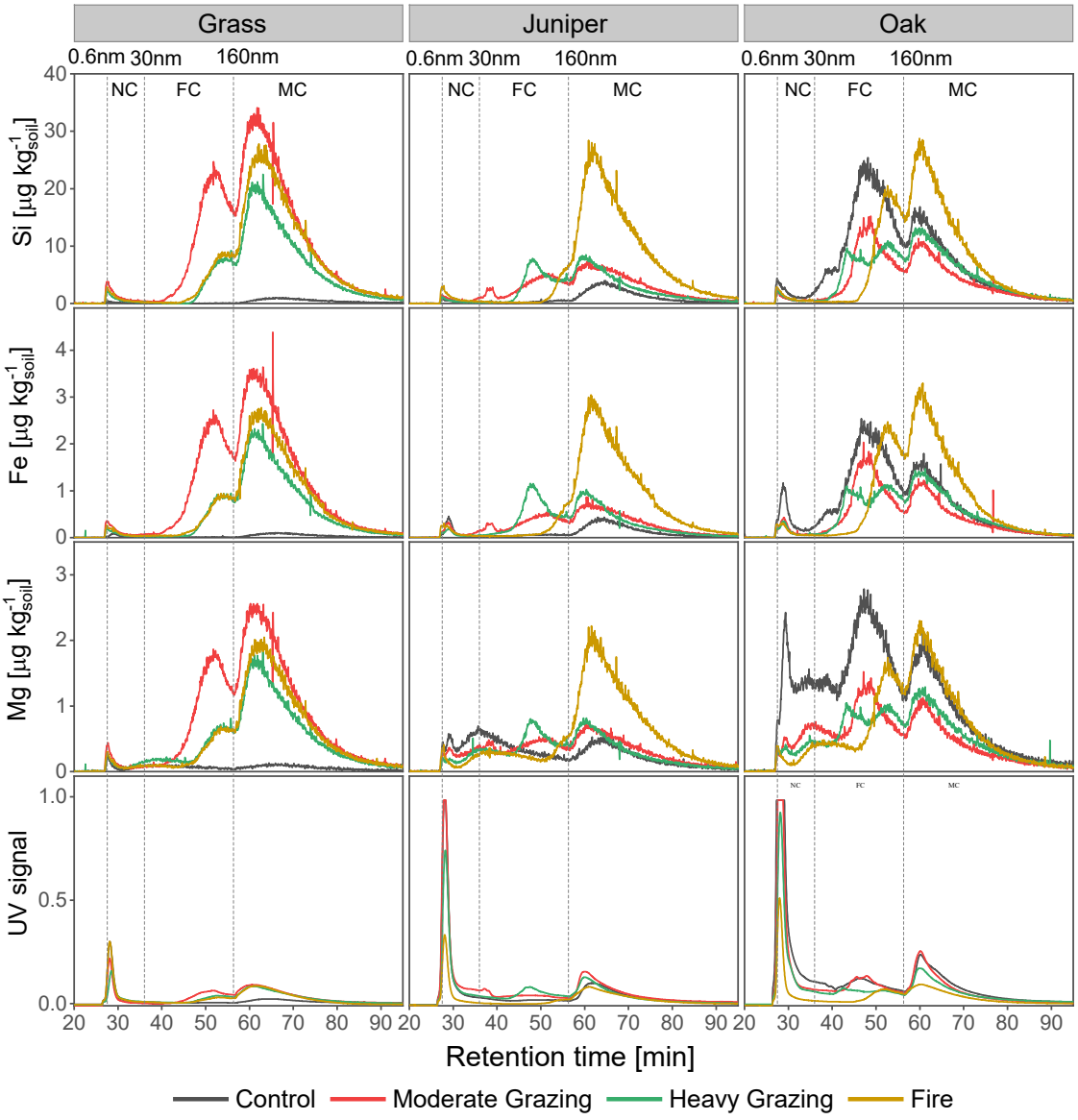

Figure S3. Concentrations of P, OC, Ca, Mg, Al, Fe and Si (mg kg_{soil}^{-1}) in water dispersible colloids (WDC, < 500 nm) and three size fraction colloids. Nanocolloids fraction (NC) are from 0.6 nm to 30 nm; Fine colloids (FC) fraction are from 30 nm to 160 nm; Medium colloids (MC) fraction are larger than 160 nm. Results of two-way ANOVAs (p-values) examining the effects of grazing, vegetation type, and their interaction are presented for the data within each graph panel. N=3. * indicates $p < 0.05$; ** indicates $p < 0.01$; ns indicates no significant difference.

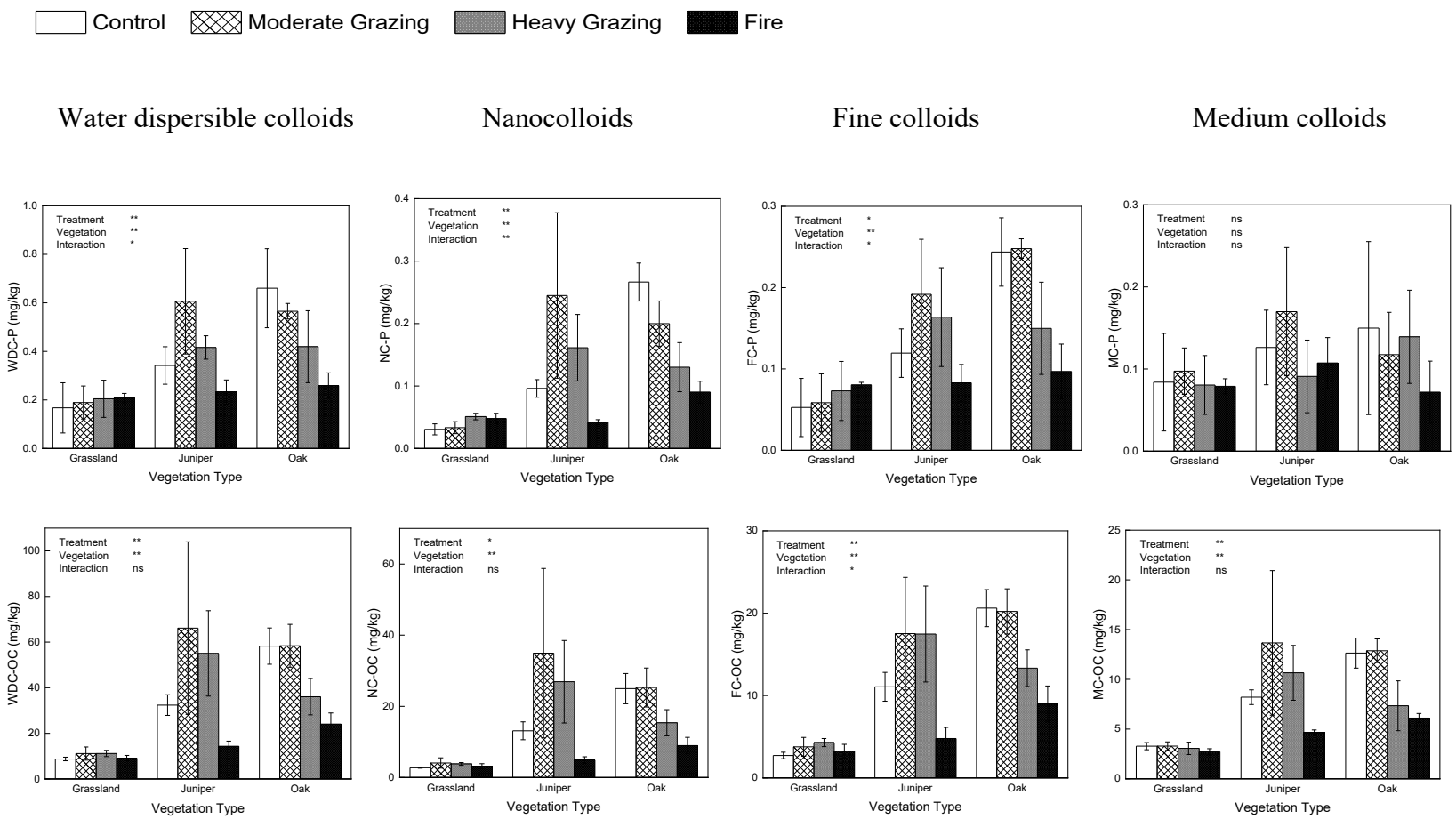

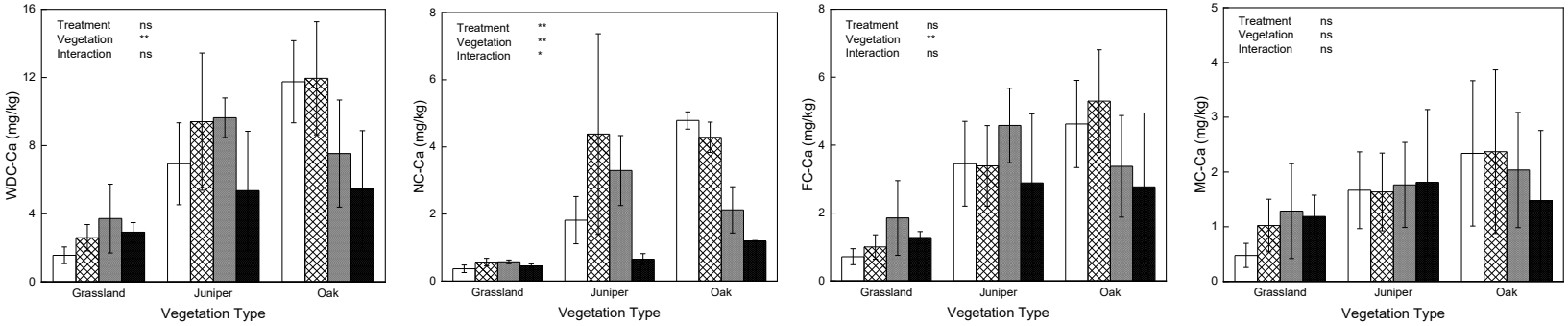
Treatment ns
Vegetation **
Interaction ns
WDC-Ca (mg/kg)
Treatment **
Vegetation **
Interaction *
NC-Ca (mg/kg)
Treatment ns
Vegetation **
Interaction ns
FC-Ca (mg/kg)
Treatment ns
Vegetation ns
Interaction ns
MC-Ca (mg/kg)
Grassland
Juniper
Oak
Vegetation Type

24

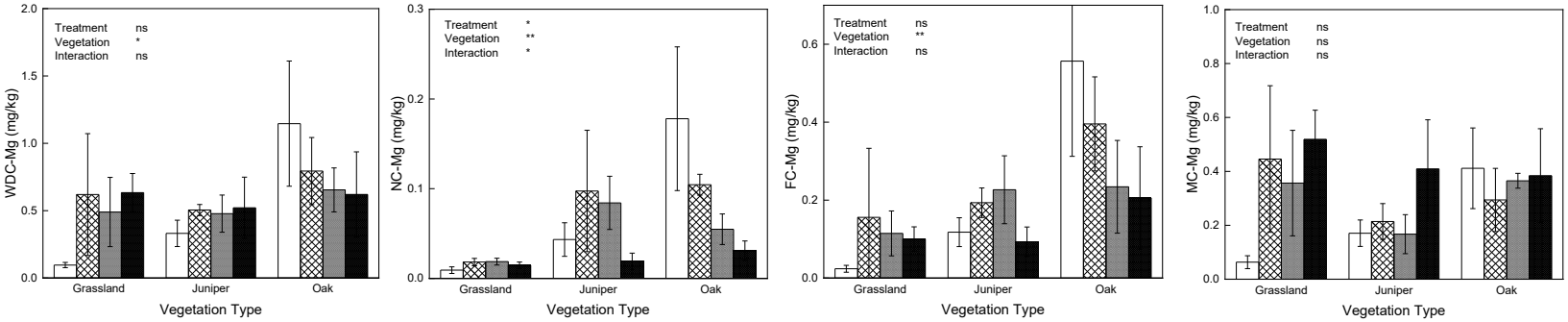
Treatment ns
Vegetation *
Interaction ns
WDC-Mg (mg/kg)
Treatment *
Vegetation **
Interaction *
NC-Mg (mg/kg)
Treatment ns
Vegetation **
Interaction ns
FC-Mg (mg/kg)
Treatment ns
Vegetation ns
Interaction ns
MC-Mg (mg/kg)
Grassland
Juniper
Oak
Vegetation Type

25

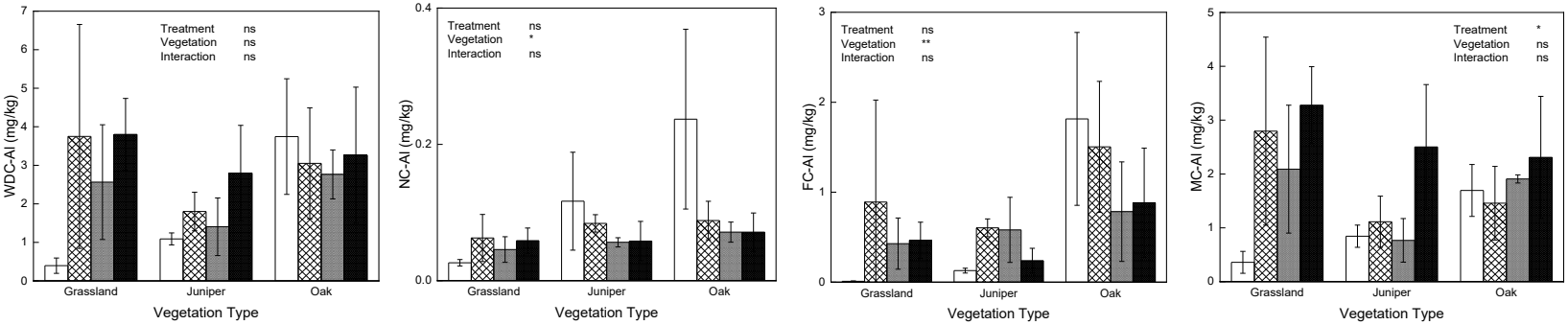
Treatment ns
Vegetation ns
Interaction ns
WDC-Al (mg/kg)
Treatment ns
Vegetation *
Interaction ns
NC-Al (mg/kg)
Treatment ns
Vegetation **
Interaction ns
FC-Al (mg/kg)
Treatment *
Vegetation ns
Interaction ns
MC-Al (mg/kg)
Grassland
Juniper
Oak
Vegetation Type

26

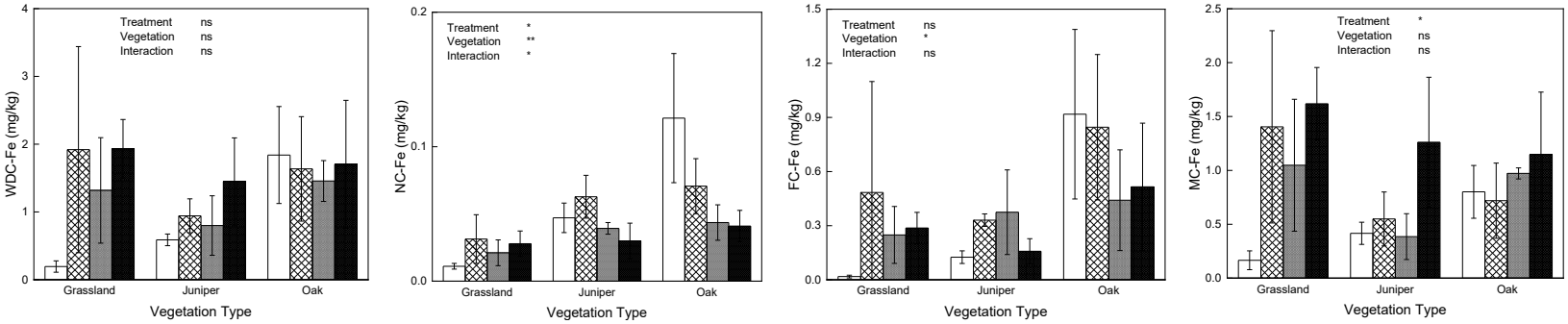
WDC-Fe (mg/kg)
NC-Fe (mg/kg)
FC-Fe (mg/kg)
MC-Fe (mg/kg)
Treatment ns
Vegetation ns
Interaction ns
Treatment *
Vegetation **
Interaction *
Treatment ns
Vegetation *
Interaction ns
Treatment *
Vegetation ns
Interaction ns
Grassland
Juniper
Oak
Vegetation Type

27

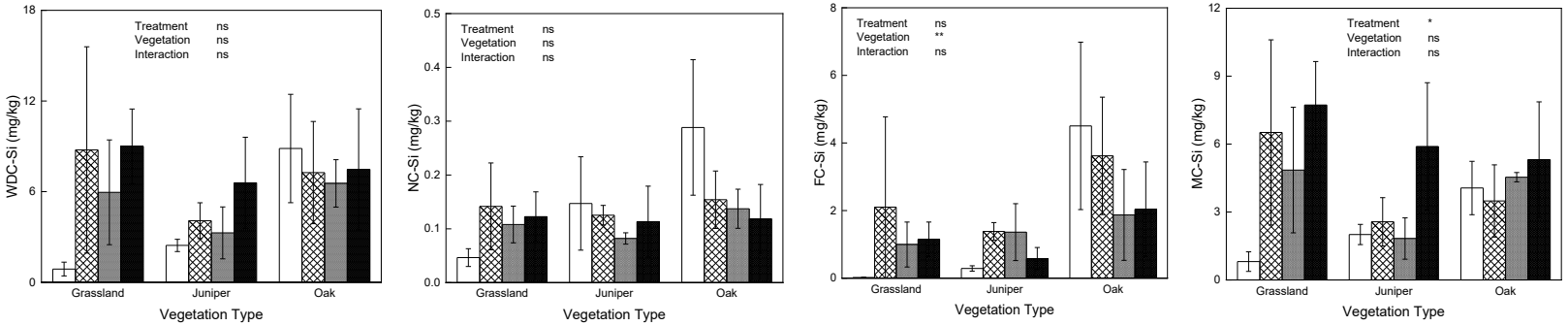
WDC-Si (mg/kg)
NC-Si (mg/kg)
FC-Si (mg/kg)
MC-Si (mg/kg)
Treatment ns
Vegetation ns
Interaction ns
Treatment ns
Vegetation **
Interaction ns
Treatment *
Vegetation ns
Interaction ns
Grassland
Juniper
Oak
Vegetation Type

28

Figure S4. ^{13}P-nuclear magnetic resonance (NMR) spectra of bulk soils, colloids (30-500 nm) and aqueous phase including colloids < 30 nm. Signal a: orthophosphate; b and d: P-Monoester; c, e, f, g, h, i, j and k: RNA hydrolysis products, P-Diester. Overlapped signal is denoted by parentheses.

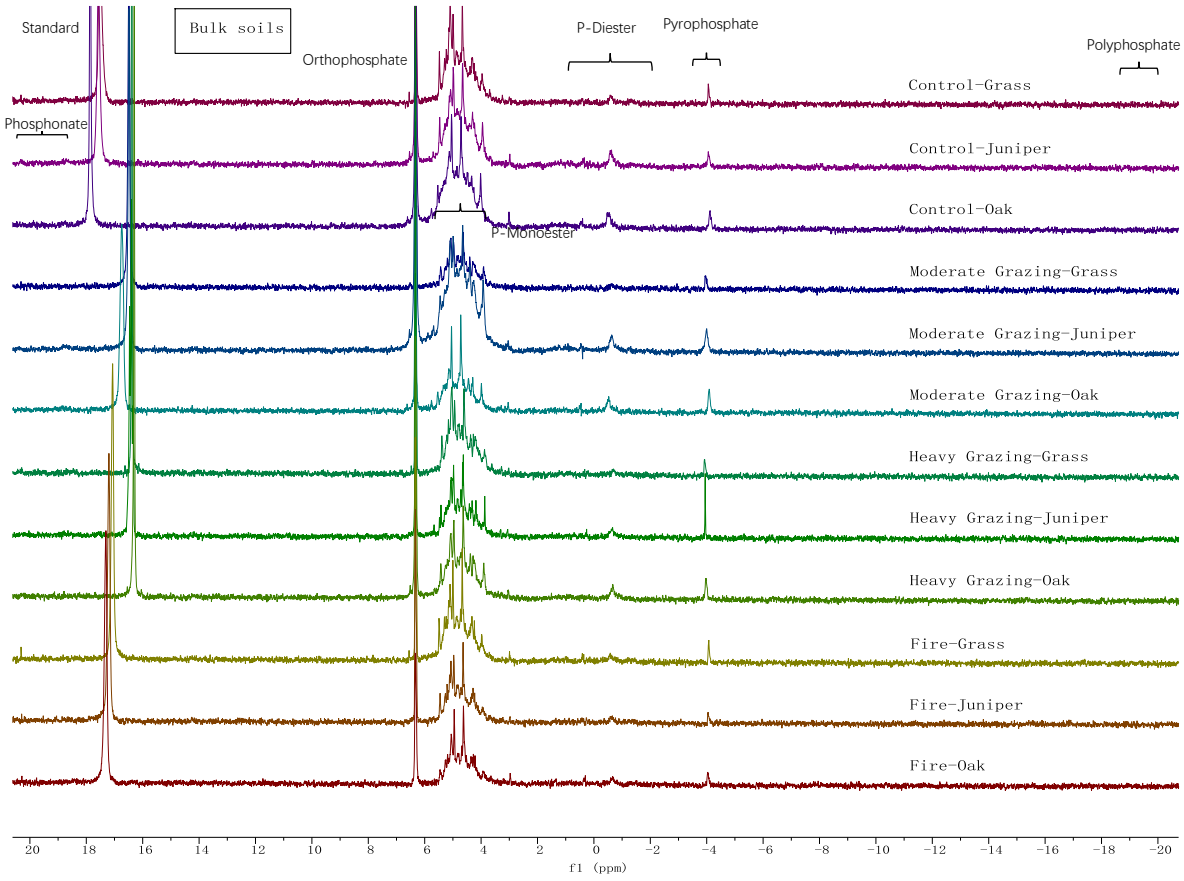

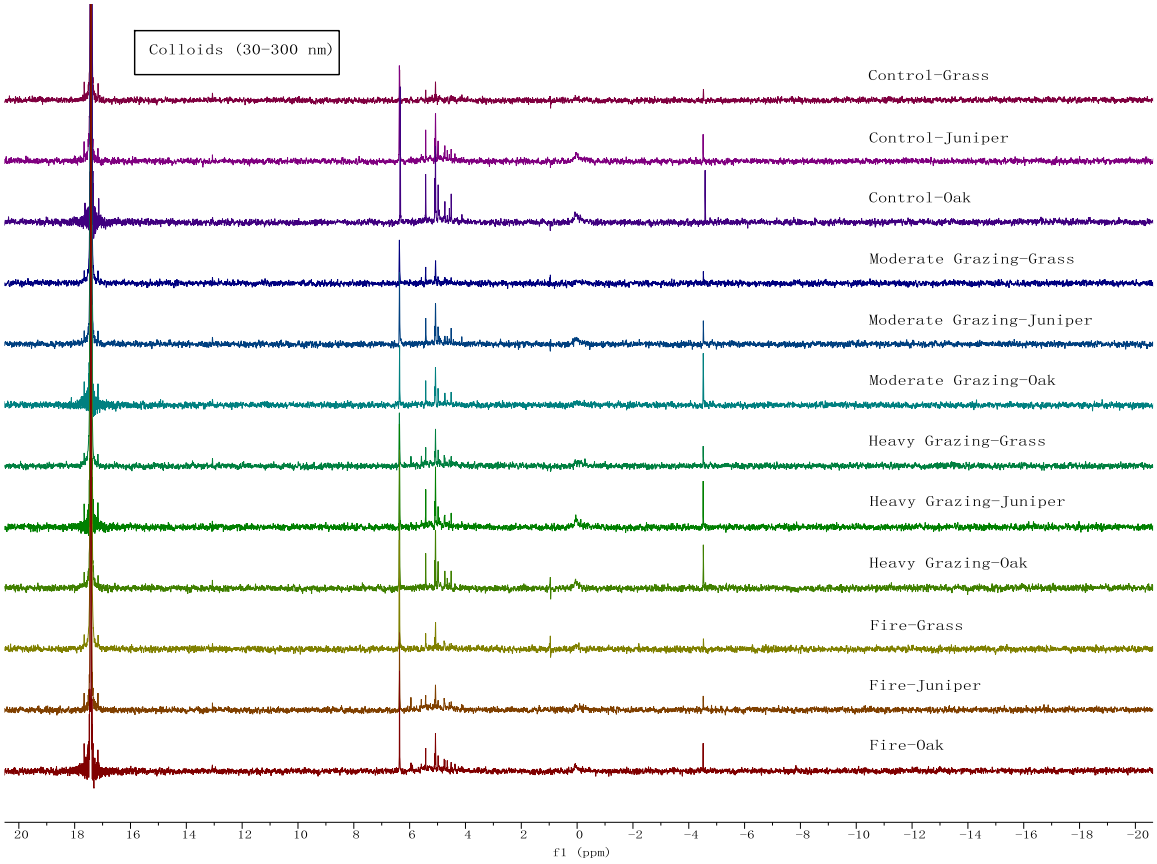
Colloids (30-300 nm)
Control-Grass
Control-Juniper
Control-Oak
Moderate Grazing-Grass
Moderate Grazing-Juniper
Moderate Grazing-Oak
Heavy Grazing-Grass
Heavy Grazing-Juniper
Heavy Grazing-Oak
Fire-Grass
Fire-Juniper
Fire-Oak
20 18 16 14 12 10 8 6 4 2 0 -2 -4 -6 -8 -10 -12 -14 -16 -18 -20
f1 (ppm)

34

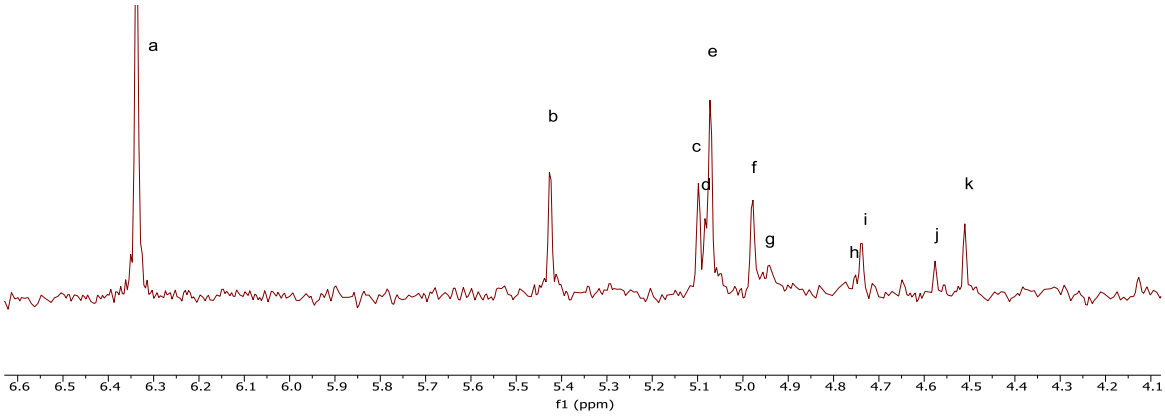
a
b
c
d
e
f
g
h
i
j
k
6.6 6.5 6.4 6.3 6.2 6.1 6.0 5.9 5.8 5.7 5.6 5.5 5.4 5.3 5.2 5.1 5.0 4.9 4.8 4.7 4.6 4.5 4.4 4.3 4.2 4.1
f1 (ppm)

35

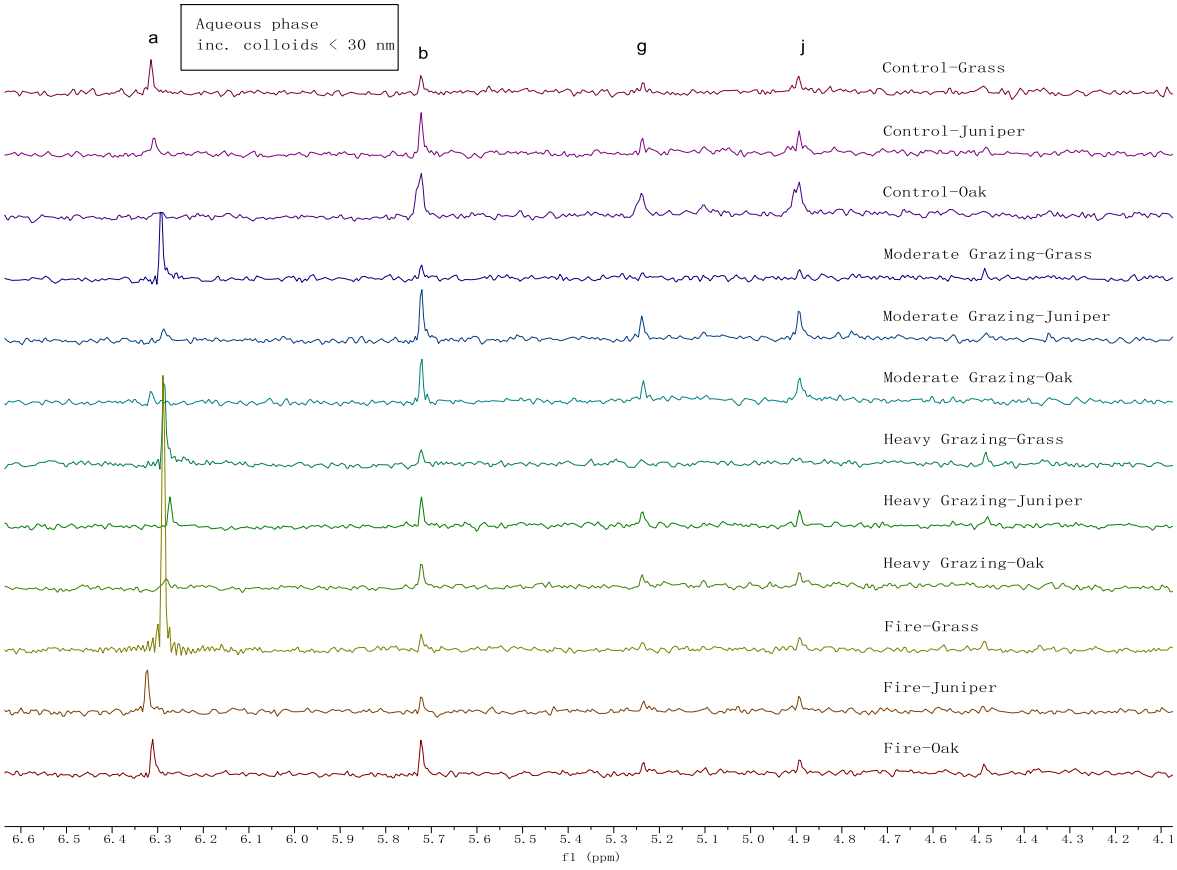
Aqueous phase
inc. colloids < 30 nm
a
b
g
j
Control-Grass
Control-Juniper
Control-Oak
Moderate Grazing-Grass
Moderate Grazing-Juniper
Moderate Grazing-Oak
Heavy Grazing-Grass
Heavy Grazing-Juniper
Heavy Grazing-Oak
Fire-Grass
Fire-Juniper
Fire-Oak
6.6 6.5 6.4 6.3 6.2 6.1 6.0 5.9 5.8 5.7 5.6 5.5 5.4 5.3 5.2 5.1 5.0 4.9 4.8 4.7 4.6 4.5 4.4 4.3 4.2 4.1
f1 (ppm)